

Nonperturbative contributions to a resummed leptonic angular distribution in inclusive neutral vector boson production

Marco Guzzi^a, Pavel M. Nadolsky^b and Bowen Wang^b

^a*Deutsches Elektronen-Synchrotron DESY,
Notkestrasse 85, 22607 Hamburg, Germany*

^b*Department of Physics, Southern Methodist University,
Dallas, TX 75275, USA*¹

Abstract

We present an analysis of nonperturbative contributions to the transverse momentum distribution of Z/γ^* bosons produced at hadron colliders. The new data on the angular distribution ϕ_η^* of Drell-Yan pairs measured at the Tevatron is shown to be in excellent agreement with a perturbative QCD prediction based on the Collins-Soper-Sterman (CSS) resummation formalism at NNLL accuracy. Using these data, we determine the nonperturbative component of the CSS resummed cross section and estimate its dependence on arbitrary resummation scales and other factors. With the scale dependence included at the NNLL level, a significant nonperturbative component is needed to describe the angular data.

¹marco.guzzi@desy.de, nadolsky@physics.smu.edu, bwang@physics.smu.edu

1 Introduction

QCD factorization methods utilizing transverse-momentum-dependent (TMD) parton distributions and fragmentation functions provide a powerful framework for describing multi-scale observables in high-energy hadron interactions. Production of Drell-Yan lepton-antilepton pairs in Z/γ^* boson production in hadron-hadron collisions is one basic process in which TMD factorization is applied to predict the boson's transverse momentum (Q_T) distribution and related angular distributions. Collinear QCD factorization is applicable for describing lepton pairs with Q_T of order of the invariant mass Q of the pair. The respective large- Q_T cross sections have been computed up to two loops in the QCD coupling strength α_s [1, 2, 3, 4] and are in reasonable agreement with the data.

But, at small Q_T , all-order resummation of large logarithms $\ln(Q_T/Q)$ needs to be performed [5, 6, 7] to obtain sensible cross sections. TMD factorization provides a systematic framework for Q_T resummation to all orders in α_s , as has been shown in classical papers by Collins, Soper, and Sterman (CSS) [8, 9, 10, 11, 12]. The resummed cross sections have been computed at various QCD orders in the CSS formalism and kindred approaches [13, 14, 15, 16, 17, 18, 19, 3, 4, 20, 21, 22]. In addition to perturbative radiative contributions, the resummed cross sections include a nonperturbative component associated with QCD dynamics at momentum scales below 1 GeV. Understanding of the nonperturbative terms is important for tests of TMD factorization and precision studies of electroweak boson production, including the measurement of W boson mass [23].

Instead of measuring Q_T distributions directly, one can measure the distribution in the angle ϕ_η^* [24] that is closely related to Q_T/Q . The ϕ_η^* distributions have been recently measured both at the Tevatron [25] and Large Hadron Collider [26, 27]. Small experimental errors of the ϕ_η^* measurements (as low as 0.5%) allow one to test the Q_T resummation formalism at an unprecedented level. On the theory side, the small- Q_T resummed form factor for Z boson production has been computed to NNLL/NNLO [28].² We would like to confront precise theoretical predictions implemented in programs LEGACY and RESBOS [29, 30, 31] by the new experimental data to obtain quantitative constraints on the nonperturbative contributions.

Such analysis is technically challenging and requires to examine several effects that were negligible in the previous studies of the resummed nonperturbative terms [29, 31, 32]. The

²Throughout the paper, “NNLO” will consistently refer to the cross sections of order α_s^2 , in accordance with the observation that the lowest-order non-zero contribution to the resummed Q_T distribution arises from the subprocess $q\bar{q} \rightarrow V$ of order α_s^0 . This is to be distinguished from an alternative convention that may be applied at large Q_T [28, 20], according to which the α_s^2 contributions are of the next-to-leading order (NLO).

framework for the fitting of Drell-Yan processes in the CSS formalism must be extended to the ϕ_η^* , rather than Q_T , distributions. Nonperturbative effects must be distinguished from comparable modifications by NNLO QCD corrections, NLO electroweak (EW) corrections, and the associated perturbative uncertainties.

To carry out this study, we modified the Q_T resummation calculation employed in our previous studies to evaluate NNLO QCD (α_s^2) and NLO EW (α_{EW}) perturbative contributions and consider the residual QCD scale dependence associated with higher-order terms. This implementation was utilized to determine the nonperturbative factor from the DØ Run-2 data on the ϕ_η^* distributions.

Our findings shed light on several questions raised in recent studies of TMD factorization [33, 34, 35, 36, 37, 38, 39, 40, 41, 42, 43, 44, 45] and soft-collinear-effective (SCET) theory [46, 47, 48]. We examine if the ϕ_η^* data corroborate the universal behavior of the resummed nonperturbative terms that is expected from the TMD factorization theorem [11] and was observed in the global analyses of Drell-Yan Q_T distributions at fixed-target and collider energies [31, 32]. We also investigate the rapidity dependence of the nonperturbative terms, which may be indicative of new types of higher-order contributions [49]. It has been argued [4, 50, 20, 21, 22] that the evidence for nonperturbative smearing is inconclusive because of a large QCD scale dependence. Since the magnitude of the scale dependence reduces with the order of the calculation, we include the dependence on the soft scales in the resummed cross section up to $\mathcal{O}(\alpha_s^2)$, *i.e.* NNLL/NNLO. In this case, the radiative contributions are estimated to the same order as in [28], either exactly or approximately, and we also include contributions responsible for the dependence on the resummation scales to one higher order (α_s^2) than in [4, 50, 20, 21, 22].

Based on our numerical implementation, we demonstrate that the impact of the power-suppressed contributions is generically distinct from the scale dependence: the nonperturbative effects can be distinguished from the NNLO scale uncertainties. The nonperturbative component that we find is consistent with a universal quadratic (Gaussian) power-suppressed contribution of the kind that may be expected on general grounds [11], and of a magnitude that is compatible with a previous global analysis of Drell-Yan Q_T distributions [32].

The DØ data are precise enough and may be able to distinguish between the Gaussian and alternative nonperturbative functions that have been recently proposed [51]. It would be insightful to examine constraints on a variety of the nonperturbative models that are currently discussed [45, 46, 44, 52], as well as the \sqrt{s} dependence of the nonperturbative contributions by using a combination of the Tevatron and LHC data. As such investigation demands significant

computational resources, it will be pursued in future work.

Our main numerical results have been reported at the QCD Evolution Workshop at Thomas Jefferson National Accelerator Facility in May 2012 [53]. The current paper documents this analysis in detail and is organized as follows. Section 2 reviews the relation between the ϕ_η^* angle and transverse momentum Q_T in the Collins-Soper-Sterman notations (Sec. 2.1), general structure of the resummed cross section and estimation of NNLO contributions and their scale dependence (Secs. 2.2, 2.3, 2.4), nonperturbative model (Sec. 2.5), matching of the small- Q_T and large- Q_T terms (Sec. 2.6), photon radiation contribution (Sec. 2.7), and numerical accuracy (Sec. 2.8). In Sec. 2.9, distinctions between the NNLL/NNLO resummed Q_T distributions obtained in the CSS formalism and the alternative approach of Refs. [82, 19, 28] are summarized.

Next, in Sec. 3, the size of the nonperturbative contributions is estimated by a χ^2 analysis of the $D\bar{O}$ data in three bins of vector boson rapidity (y_Z), by applying two different methods to examine the scale dependence of the resummed cross section. By using the constraining power of this data set, we suggest a Gaussian smearing factor suitable for W and Z production, and we give an estimate at 68% C.L. for the leading parameter of the NP functional form. We provide the user with several sets of grids of theory predictions for phenomenological applications based on CT10 NNLO [54] PDF eigenvector sets, and for scans of the nonperturbative smearing function and estimates of its uncertainty in future measurements.

2 Overview of the resummation method

2.1 Relation between Q_T and ϕ_η^* variables

The Collins-Soper-Sterman (CSS) resummation formalism predicts fully differential distributions in electroweak boson production, including decay of heavy bosons. While the original formulation of the CSS formalism deals with resummation of logarithms dependent on the boson's transverse momentum Q_T , it can be readily extended to resum angular variables of decay particles. One such variable is the azimuthal angle separation $\Delta\varphi$ of the leptons in the lab frame, which approaches π (back-to-back production of leptons in the transverse plane) when $Q_T \rightarrow 0$. Consequently, the region $\Delta\varphi \rightarrow \pi$ is sensitive to small- Q_T resummation [30].

Recently, an angular variable ϕ_η^* was proposed in [24] that has an experimental advantage compared to Q_T and $\Delta\varphi$. The ϕ_η^* variable is not affected by the experimental resolution on the magnitudes of the leptons' (transverse) momenta that limits the accuracy of the Q_T measurement. Soft and collinear resummation for the ϕ_η^* distribution can be worked out either analytically [20, 21, 50, 22] or numerically by integrating the resummed Q_T distribution over

the leptons' phase space.

To describe decays of massive bosons, the CSS formalism [30] usually operates with the lepton polar angle θ_{CS} and azimuthal angle φ_{CS} in the Collins-Soper (CS) reference frame [55]. The CS frame is a rest frame of the vector boson in which the z axis bisects the angle formed by the momenta \vec{p}_1 and $-\vec{p}_2$ of the incident quark and antiquark. In the CS frame, the decay leptons escape back-to-back ($\vec{l}_1 + \vec{l}_2 = 0$), and the electron's and positron's 4-momenta are

$$l_1^\mu|_{\text{CS frame}} = (Q/2) \{1, \cos \varphi_{CS} \sin \theta_{CS}, \sin \varphi_{CS} \sin \theta_{CS}, \cos \theta_{CS}\}, \quad (1)$$

and

$$l_2^\mu|_{\text{CS frame}} = (Q/2) \{1, -\cos \varphi_{CS} \sin \theta_{CS}, -\sin \varphi_{CS} \sin \theta_{CS}, -\cos \theta_{CS}\}. \quad (2)$$

On the other hand, the angular variable ϕ_η^* is defined in a different frame (“ η frame”), in which the leptons escape θ_η^* and $\pi - \theta_\eta^*$ with respect to the incident beams direction. The η frame is related to the lab frame by a boost $\beta = \tanh((\eta_1 + \eta_2)/2)$ along the incident beam direction, where η_1 and η_2 are the pseudorapidities of e^- and e^+ in the lab frame. The frame coincides with the CS frame when $Q_T = 0$. Knowing the polar angle θ_η^* in the η frame and the difference $\Delta\varphi = \varphi_1 - \varphi_2$ of the lepton's azimuthal angles in the transverse plane to the beam direction, one defines

$$\phi_\eta^* = \tan(\phi_{acop}/2) \sin \theta_\eta^* \quad (3)$$

in terms of the acoplanarity angle $\phi_{acop} = \pi - \Delta\varphi$. We write $\cos \theta_\eta^*$ as a function of the lepton momenta in the lab frame as

$$\cos \theta_\eta^* = \tanh\left(\frac{\eta_1 - \eta_2}{2}\right) = \frac{\sqrt{l_1^+ l_2^-} - \sqrt{l_1^- l_2^+}}{\sqrt{l_1^+ l_2^-} + \sqrt{l_1^- l_2^+}} = \frac{f(\cos \theta_{CS}) - f(-\cos \theta_{CS})}{f(\cos \theta_{CS}) + f(-\cos \theta_{CS})}, \quad (4)$$

where $l_{1,2}^\pm = (l_{1,2}^0 \pm l_{1,2}^z)/\sqrt{2}$,

$$f(\cos \theta_{CS}) \equiv \sqrt{M_T^2 + 2M_T Q \cos \theta_{CS} + Q^2 \cos^2 \theta_{CS} - Q_T^2 \sin^2 \theta_{CS} \cos^2 \varphi_{CS}}, \quad (5)$$

and $M_T^2 = Q^2 + Q_T^2$. We also write $\cos \Delta\varphi$ as

$$\begin{aligned} \cos \Delta\varphi &= (Q_T^2 - Q^2 \sin^2 \theta_{CS} - Q_T^2 \sin^2 \theta_{CS} \cos^2 \varphi_{CS}) \\ &\times [(Q^2 \sin^2 \theta_{CS} + Q_T^2 \sin^2 \theta_{CS} \cos^2 \varphi_{CS} + Q_T^2)^2 - 4M_T^2 Q_T^2 \sin^2 \theta_{CS} \cos^2 \varphi_{CS}]^{-\frac{1}{2}}. \end{aligned} \quad (6)$$

In the limit $Q_T \rightarrow 0$, ϕ_η^* simplifies to

$$\phi_\eta^* \approx (Q_T/Q) \sin \varphi_{CS}, \quad (7)$$

since $\tan(\phi_{acop}/2) = \sqrt{(1 + \cos \Delta\varphi) / (1 - \cos \Delta\varphi)}$, and

$$\theta_\eta^* \rightarrow \theta_{CS}, \quad \cos \Delta\varphi \rightarrow -1 + 2 \left(\frac{Q_T \sin \varphi_{CS}}{Q \sin \theta_{CS}} \right)^2. \quad (8)$$

Measurement of ϕ_η^* thus directly probes Q_T/Q .³

Relations like these can analytically express the ϕ_η^* distribution in terms of the Q_T distribution, but in practice it is easier to compute the ϕ_η^* distribution by Monte-Carlo integration in RESBOS code. In this case, the interval of small Q_T/Q maps onto the region of small ϕ_η^* . For example, in Z production at $Q \approx M_Z$, the range $10^{-3} \leq \phi_\eta^* \leq 0.5$ radians corresponds to $0.1 \lesssim Q_T \lesssim 50$ GeV.

2.2 General structure of the resummed cross section

The resummed cross sections that we present are based on the calculation in [13, 29, 30, 31] with added higher-order radiative contributions (Secs. 2.3, 2.4) and modified nonperturbative model (Sec. 2.5). We write the fully differential cross section for Z boson production and decay as

$$\frac{d\sigma(h_1 h_2 \rightarrow (Z \rightarrow \ell \bar{\ell}) X)}{dQ^2 dy_Z dQ_T^2 d\cos\theta_{CS} d\varphi_{CS}} = \sum_{\alpha=-1}^4 F_\alpha(Q, Q_T, y) A_\alpha(\theta_{CS}, \varphi_{CS}) \quad (9)$$

in terms of the structure functions $F_\alpha(Q, Q_T, y_Z)$ and angular functions $A_\alpha(\theta_{CS}, \varphi_{CS})$. The variables Q , Q_T , and y_Z correspond to the invariant mass, transverse momentum, and rapidity of the boson in the lab frame; θ_{CS} and φ_{CS} are the lepton decay angles in the CS frame. Among the structure functions F_α , two (associated with the angular functions $A_{-1} = 1 + \cos^2 \theta_{CS}$ and $A_3 = 2 \cos \theta_{CS}$) include resummation of soft and collinear logarithms in the small- Q_T limit. For such functions, we write

$$F_\alpha(Q, Q_T, y_Z) = W_\alpha(Q, Q_T, y_Z; C_1/b, C_2 Q, C_3/b) + Y_\alpha(Q, Q_T, y_Z; C_4 Q), \quad (10)$$

where

$$W_\alpha(Q, Q_T, y_Z) = \int \frac{d^2 b}{4\pi^2} e^{i\vec{Q}_T \cdot \vec{b}} \sum_{j=u,d,s,\dots} \widetilde{W}_{\alpha,j}(b, Q, y_Z) \quad (11)$$

is introduced to resum small- Q_T logarithms to all orders in α_s . The W term depends on several auxiliary QCD scales C_1/b , $C_2 Q$, and C_3/b with constant coefficients $C_{1,2,3} \approx 1$ that emerge

³The asymptotic relation between ϕ_η^* and Q_T/Q can alternatively be obtained by introducing the component a_T of \vec{Q}_T along the thrust axis $\hat{n} = (\vec{l}_{1,T} - \vec{l}_{2,T}) / |\vec{l}_{1,T} - \vec{l}_{2,T}|$, where $\vec{l}_{1,T}$ and $\vec{l}_{2,T}$ are the transverse momenta of e^- and e^+ , and identifying $a_T = Q_T \sin \varphi_{CS}$ at $Q_T \rightarrow 0$ [21, 22, 24, 56].

from the solution of differential equations describing renormalization and gauge invariance of Q_T distributions [8, 12]. $Y_\alpha(Q, Q_T, y_Z; C_4 Q)$ is a part of the non-singular remainder, or “the Y term”. It depends on a factorization and renormalization momentum scale $C_4 Q$.

The Fourier-Bessel integral over the transverse position b in the W term in Eq. (11) acquires contributions from the region of small transverse positions $0 \leq b \lesssim 1 \text{ GeV}^{-1}$, where the form factor can be approximated in perturbative QCD, and the region $b \gtrsim 1 \text{ GeV}^{-1}$, where the perturbative expansion in the QCD coupling $\alpha_s(1/b)$ breaks down, and nonperturbative methods are necessitated. In Z boson production, the small- b perturbative contribution dominates the Fourier-Bessel integral for any Q_T value [7, 32, 57]. At Q_T below 5 GeV, the production rate is also mildly sensitive to the behavior in the $b > 0.5 \text{ GeV}^{-1}$ interval, where the full expression for $\widetilde{W}_{\alpha,j}(b, Q)$ is yet unknown.

To determine the acceptable large- b forms of $\widetilde{W}_{\alpha,j}(b, Q)$ by comparison to the latest Z boson data, we need to update the leading-power contribution to $\widetilde{W}_{\alpha,j}(b, Q, y_Z)$ computable in perturbative QCD, denoted by $\widetilde{W}_{\alpha,j}^{pert}(b, Q, y_Z)$, by considering additional QCD and electromagnetic corrections and dependence on QCD factorization scales. In particular, scale dependence in the perturbative form factor \widetilde{W}^{pert} may smear the sensitivity to the nonperturbative factor [3, 20, 28, 50]. We will review the perturbative contributions in the next two subsections.

2.3 Perturbative coefficients for canonical scales

For a particular “canonical” combination of the scale parameters, the perturbative contributions simplify; the resummed form factor at $b \ll 1 \text{ GeV}^{-1}$ takes the form

$$\begin{aligned} \widetilde{W}_{\alpha,j}^{pert}(b, Q, y_Z) &= \sum_{j=u,d,s,\dots} |H_{\alpha,j}(Q, \Omega)|^2 \exp[-S(b, Q)] \\ &\times \sum_{a=g,q,\bar{q}} [C_{ja} \otimes f_{a/h_1}](\chi_1, \mu_F) \sum_{b=g,q,\bar{q}} [C_{\bar{j}b} \otimes f_{b/h_2}](\chi_2, \mu_F) \end{aligned} \quad (12)$$

in terms of a $2 \rightarrow 2$ hard part $|H_{\alpha,j}(Q, \Omega)|^2$, Sudakov integral

$$S(b, Q) = \int_{b_0^2/b^2}^{Q^2} \frac{d\bar{\mu}^2}{\bar{\mu}^2} \left[A(\bar{\mu}) \ln \left(\frac{Q^2}{\bar{\mu}^2} \right) + B(\bar{\mu}) \right], \quad (13)$$

and convolutions $[C_{j/a} \otimes f_{a/h}]$ of Wilson coefficient functions $C_{j/a}$ and PDFs $f_{a/h}$ for a parton a inside the initial-state hadron h . The convolution integral is defined by

$$[C_{ja} \otimes f_{a/h}](\chi, \mu_F) = \int_x^1 \frac{d\xi}{\xi} C_{ja} \left(\frac{\chi}{\xi}, \mu_F \right) f_{a/h}(\xi, \mu_F). \quad (14)$$

In Eq. (14) the convolution depends on the momentum fractions $\chi_{1,2}$ that reduce to $x_{1,2}^{(0)} \equiv (Q/\sqrt{s})e^{\pm y_Z}$ in the limit $Q_T^2/Q^2 \rightarrow 0$, as explained in Sec. 2.6, as well as on the factorization

scale $\mu_F = b_0/b$. Some scales are proportional to the constant $b_0 = 2e^{-\gamma_E} = 1.123\dots$, where $\gamma_E = 0.577\dots$ is the Euler-Mascheroni constant.

The functions $H_{\alpha,j}$, A , B , and C can be expanded as a series in the QCD coupling strength,

$$H_{\alpha,j}(Q, \Omega; \alpha_s(\bar{\mu})) = 1 + \sum_{n=1}^{\infty} \left(\frac{\alpha_s(\bar{\mu})}{\pi} \right)^n H_{\alpha,j}^{(n)}(Q, \Omega), \quad A(\alpha_s(\bar{\mu})) = \sum_{n=1}^{\infty} \left(\frac{\alpha_s(\bar{\mu})}{\pi} \right)^n A^{(n)}, \text{ etc.} \quad (15)$$

Some perturbative contributions can be moved between the hard function $H_{\alpha,j}$ and Sudakov exponential depending on the resummation scheme [16]. In the Collins-Soper-Sterman (CSS) resummation scheme, $H_{\alpha,j}(\alpha_s) = 1$ to all α_s orders. In the Catani-De Florian-Grazzini (CFG) resummation scheme, $H_{\alpha,j}(\alpha_s)$ includes hard virtual contributions starting at $\mathcal{O}(\alpha_s)$, while the Sudakov exponential depends only on the type of the initial-state particle (quark or gluon) that radiates soft emissions. In Drell-Yan production, differences between the CSS and CFG schemes are small, below 1% in the kinematic region explored. We carry out the analysis in the CSS scheme, but the nonperturbative function that we obtain can be readily used with the CFG scheme.

The functions A and B for the canonical choice of scales are evaluated up to $\mathcal{O}(\alpha_s^3)$ and $\mathcal{O}(\alpha_s^2)$ respectively, using their known perturbative coefficients [58, 59, 60, 61, 62, 63]. The three-loop coefficient $A^{(3)}$ is included, but has a weak effect on the cross section (3% at $Q_T \approx 2$ GeV). The coefficient $A^{(3)}$ has been derived within the soft-collinear effective theory [64] and found to contain a term arising from the ‘‘collinear anomaly’’, besides the $\mathcal{O}(\alpha_s^3)$ cusp contribution known from [63]. The ‘‘collinear’’ anomaly contribution breaks the symmetry of the SCET Lagrangian by regulators of loop integrals [64, 65, 66, 67]. The expansion of \widetilde{W}^{pert} in the CSS scheme, is found to be in agreement with that derived in SCET up to NLO. We checked that $A_{SCET}^{(3)}$ has inappreciable influence on the conclusions.

The Wilson coefficient functions $\mathcal{C}^{(i)}$ are computed exactly up to $\mathcal{O}(\alpha_s)$ and approximately to $\mathcal{O}(\alpha_s^2)$. Most of our numerical results were obtained with the $\mathcal{O}(\alpha_s^2)$ approximation for the Wilson coefficient before the exact $\mathcal{O}(\alpha_s^2)$ result were published [4, 3, 28]. This expression is constructed by using a numerical approximation for the canonical part of the Wilson coefficient at $\mathcal{O}(\alpha_s^2)$ and exact expression for its dependence on soft scales. Our *a posteriori* comparison shows the approximation to be close to the exact expression, cf. the next subsection.

The Y contribution in Eq. (11) is defined as the difference between the fixed-order perturbative Q_T distribution calculation and the asymptotic distribution obtained by expanding the

perturbative part \widetilde{W}^{pert} up to the same order. It is given by

$$Y_\alpha(Q_T, Q, y_Z) = \int \frac{d\xi_1}{\xi_1} \int \frac{d\xi_2}{\xi_2} \sum_{n=1}^{\infty} \left[\frac{\alpha_s(C_4 Q)}{\pi} \right]^n \times \\ f_{a/h_1}(\xi_1, C_4 Q) R_{\alpha, ab}^{(n)}(Q_T, Q, y_Z; \xi_1, \xi_2, C_4 Q) f_{b/h_2}(\xi_2, C_4 Q), \quad (16)$$

where the functions $R_{\alpha, ab}^{(n)}$ are integrable when $Q_T \rightarrow 0$, and their explicit expressions for all contributing α to $\mathcal{O}(\alpha_s)$ can be found in [10, 30]. The $\mathcal{O}(\alpha_s^2)$ contribution to the dominant structure function Y_{-1} is included using the calculation in [1, 57]. $\mathcal{O}(\alpha_s^2)$ corrections to the other structure functions in the Y term are essentially negligible in the small- Q_T region of our fit.

2.4 Perturbative coefficients for arbitrary scales

The resummed form factor in Eq. (12) can be generalized to allow variations in the arbitrary factorization scales arising in the solution of Collins-Soper differential equations. At small b , the scale-dependent expression takes the form

$$\widetilde{W}_{\alpha, j}^{pert} = \sum_{j=u, d, s, \dots} |H_{\alpha, j}(Q, \Omega, C_2 Q)|^2 \exp \left[- \int_{C_1^2/b^2}^{C_2^2 Q^2} \frac{d\bar{\mu}^2}{\bar{\mu}^2} A(\bar{\mu}; C_1) \ln \left(\frac{C_2^2 Q^2}{\bar{\mu}^2} \right) + B(\bar{\mu}; C_1, C_2) \right] \\ \times \sum_{a=g, q, \bar{q}} [C_{ja} \otimes f_{a/h_1}] \left(\chi_1, \frac{C_1}{C_2}, \frac{C_3}{b} \right) \sum_{b=g, q, \bar{q}} [C_{\bar{j}b} \otimes f_{b/h_2}] \left(\chi_2, \frac{C_1}{C_2}, \frac{C_3}{b} \right), \quad (17)$$

where the coefficients $C_1 = b\bar{\mu}$ and $C_2 = \bar{\mu}/Q$ are associated with the lower and upper integration limits in Eq. (17), while $\mu_F = C_3/b$ is the factorization scale at which Wilson coefficient functions are evaluated. The ‘‘canonical’’ representation adopted in Eq. (12) corresponds to $C_1 = C_3 = b_0$ and $C_2 = 1$. For the rest of the discussion, we use the same scale $C_2 Q$ to compute the hard function $H_{\alpha, j}$ and the Y term, *i.e.* set $C_4 = C_2$.

The perturbative coefficients $A^{(n)}$, $B^{(n)}$, and $C^{(n)}$ are generally dependent on the scale coefficients, but the full form factor \widetilde{W}^{pert} is independent when expanded to a fixed order in α_s . We can therefore reconstruct the perturbative coefficients order-by-order for arbitrary C_1 , C_2 , C_3 if we know the canonical values of the coefficients, indicated by the superscript ‘‘(c)’’.

By truncating the series at $\mathcal{O}(\alpha_s^2)$, we must have

$$\widetilde{W}(b, Q, C_1, C_2, C_3)|_{\mathcal{O}(\alpha_s^2)} = \widetilde{W}(b, Q, C_1 = C_3 = b_0, C_2 = 1)|_{\mathcal{O}(\alpha_s^2)}. \quad (18)$$

Making a series expansion on both sides of Eq. (18), we find the following relations by equating

the coefficients in front of each power of $\log(b^2 Q^2)$:

$$A^{(1)}(C_1) = A^{(1,c)}; \quad (19)$$

$$A^{(2)}(C_1) = A^{(2,c)} - A^{(1,c)}\beta_0 \ln \frac{b_0}{C_1}; \quad (20)$$

$$A^{(3)}(C_1) = A^{(3,c)} - 2A^{(2,c)}\beta_0 \ln \frac{b_0}{C_1} - \frac{A^{(1,c)}}{2}\beta_1 \ln \frac{b_0}{C_1} + A^{(1,c)}\beta_0^2 \left(\ln \frac{b_0}{C_1} \right)^2; \quad (21)$$

$$B^{(1)}(C_1, C_2) = B^{(1,c)} - A^{(1,c)} \ln \frac{b_0^2 C_2^2}{C_1^2}; \quad (22)$$

$$B^{(2)}(C_1, C_2) = B^{(2,c)} - A^{(2,c)} \ln \frac{b_0^2 C_2^2}{C_1^2} + \beta_0 \left[A^{(1,c)} \ln^2 \frac{b_0}{C_1} + B^{(1,c)} \ln C_2 - A^{(1,c)} \ln^2 C_2 \right]; \quad (23)$$

$$\begin{aligned} \mathcal{C}_{ja}^{(1)} \left(\xi, \frac{C_1}{C_2}, C_3 \right) &= \mathcal{C}_{ja}^{(1,c)}(\xi) + \delta_{ja} \delta(1-\xi) \left\{ \frac{B^{(1,c)}}{2} \ln \frac{b_0^2 C_2^2}{C_1^2} - \frac{A^{(1,c)}}{4} \left(\ln \frac{b_0^2 C_2^2}{C_1^2} \right)^2 \right\} \\ &\quad - P_{ja}^{(1)}(x) \ln \frac{\mu_F b}{b_0}; \end{aligned} \quad (24)$$

$$\begin{aligned} \mathcal{C}_{ja}^{(2)} \left(\xi, \frac{C_1}{C_2}, C_3 \right) &= \mathcal{C}_{ja}^{(2,c)}(\xi) + \delta_{ja} \delta(1-\xi) L^{(2)}(C_1, C_2) \\ &\quad + \left\{ \frac{\beta_0}{2} \mathcal{C}_{jb}^{(1,c)}(\xi) - [\mathcal{C}_{jb}^{(1,c)} \otimes P_{ba}^{(1)}](\xi) - P_{ja}^{(2)}(\xi) \right\} \ln \frac{\mu_F b}{b_0} \\ &\quad + \frac{1}{2} [P_{jb}^{(1)} \otimes P_{ba}^{(1)}](\xi) \ln^2 \frac{\mu_F b}{b_0}. \end{aligned} \quad (25)$$

Here the beta-function coefficients for N_c colors and N_f flavors are $\beta_0 = (11N_c - 2N_f)/6$, $\beta_1 = (17N_c^2 - 5N_c N_f - 3C_F N_f)/6$, $C_F = (N_c^2 - 1)/(2N_c)$. $P_{ja}^{(n)}(\xi)$ is a splitting function of order n . The term $L^{(2)}(C_1, C_2)$ in $\mathcal{C}_{ja}^{(2)}$ realizes the exact dependence on the *soft* scale constants C_1 and C_2 :

$$\begin{aligned} L^{(2)}(C_1, C_2) &\equiv \frac{1}{32} (A^{(1,c)})^2 \log^4 \left(\frac{b_0^2 C_2^2}{C_1^2} \right) \\ &\quad - \frac{1}{8} A^{(1,c)} \beta_0 \log \left(\frac{b^2 \mu_F^2}{b_0^2} \right) \log^2 \left(\frac{b_0^2 C_2^2}{C_1^2} \right) - \frac{1}{8} A^{(1,c)} B^{(1,c)} \log^3 \left(\frac{b_0^2 C_2^2}{C_1^2} \right) \\ &\quad - \frac{1}{24} A^{(1,c)} \beta_0 \log^3 \left(\frac{b_0^2 C_2^2}{C_1^2} \right) - \frac{1}{4} A^{(1,c)} \delta \mathcal{C}_{1c} \log^2 \left(\frac{b_0^2 C_2^2}{C_1^2} \right) \\ &\quad - \frac{1}{4} A^{(2,c)} \log^2 \left(\frac{b_0^2 C_2^2}{C_1^2} \right) + \frac{1}{4} \beta_0 B^{(1,c)} \log \left(\frac{b^2 \mu_F^2}{b_0^2} \right) \log \left(\frac{b_0^2 C_2^2}{C_1^2} \right) \\ &\quad + \frac{1}{8} (B^{(1,c)})^2 \log^2 \left(\frac{b_0^2 C_2^2}{C_1^2} \right) + \frac{1}{8} \beta_0 B^{(1,c)} \log^2 \left(\frac{b_0^2 C_2^2}{C_1^2} \right) \\ &\quad + \frac{1}{2} B^{(1,c)} \delta \mathcal{C}_{1c} \log \left(\frac{b_0^2 C_2^2}{C_1^2} \right) + \frac{1}{2} B^{(2,c)} \log \left(\frac{b_0^2 C_2^2}{C_1^2} \right). \end{aligned} \quad (26)$$

The dependence on C_3 is small already at $\mathcal{O}(\alpha_s)$. The canonical coefficients in the CSS scheme are [30]

$$\begin{aligned} A^{(1,c)} &= C_F; & B^{(1,c)} &= -\frac{3}{2}C_F; & A^{(2,c)} &= C_F \left[\left(\frac{67}{36} - \frac{\pi^2}{12} \right) C_A - \frac{5}{18}N_f \right]; \\ B^{(2,c)} &= C_F^2 \left(\frac{\pi^2}{4} - \frac{3}{16} - 3\zeta_3 \right) + C_A C_F \left(\frac{11}{36}\pi^2 - \frac{193}{48} + \frac{3}{2}\zeta_3 \right) + \frac{1}{2}C_F N_f \left(-\frac{\pi^2}{9} + \frac{17}{12} \right), \end{aligned} \quad (27)$$

and $\delta\mathcal{C}^{(1,c)} = -\ln^2(C_1/(b_0 C_2)e^{-3/4}) + \pi^2/4 - 23/16$.

The expression for $\mathcal{C}_{ja}^{(2)}(\xi, C_1/C_2, C_3)$ in Eq. (25) is more complex than the one for the other coefficients. From the fixed-order NNLO calculation [68] we know that the contribution $\mathcal{C}_{ja}^{(2)}$ is small in magnitude (2-3% of the cross section) in Z production and does not vary strongly with y_Z [2], hence has weak dependence on ξ . Its importance is further reduced in the computation of the *normalized* ϕ_η^* distributions that we will work with.

Knowing this, we approximate $\mathcal{C}_{ja}^{(2)}(\xi, C_1/C_2, C_3)$ as

$$\mathcal{C}_{ja}^{(2)}(\xi, C_1/C_2, C_3) \approx \left\{ \langle \delta\mathcal{C}^{(2,c)} \rangle + L^{(2)}(C_1, C_2) \right\} \delta(1-\xi) \delta_{ja}, \quad (28)$$

where $\langle \delta\mathcal{C}^{(2,c)} \rangle$ denotes the average value of the Wilson coefficient in Z production for the canonical scale combination and $L^{(2)}(C_1, C_2)$ is the same as in Eq.(26). It is estimated from the requirement that the resummed cross section reproduces the fixed-order prediction for the computation of the invariant mass distribution, which is known since a long time [69] and was evaluated in our analysis by the computer code CANDIA [70, 71]⁴. The second term in Eq. (28) realizes the exact dependence on *soft* scale constants C_1 and C_2 . The ξ dependence of $\mathcal{C}_{ja}^{(2)}(\xi, C_1/C_2, C_3)$ is neglected in this approximation. The C_3 dependence is included to $\mathcal{O}(\alpha_s)$ and is of the same order as the $\mathcal{O}(\alpha_s^2)$ dependence on C_1 and C_2 .

The part $\delta\mathcal{C}_{ja}^{(2,c)}$ of $\mathcal{C}_{ja}^{(2,c)}$ proportional to $\delta_{ja}\delta(1-\xi)$ can be determined from the calculation in [28] as

$$\begin{aligned} \delta\mathcal{C}_{qq,c}^{(2)} &= C_A C_F \left(\frac{59}{18}\zeta_3 - \frac{1535}{192} + \frac{215}{216}\pi^2 - \frac{\pi^4}{240} \right) + \frac{1}{4}C_F^2 \left(-15\zeta_3 + \frac{511}{16} - \frac{67\pi^2}{12} + \frac{17}{45}\pi^4 \right) \\ &\quad - \frac{1}{16}(\pi^2 - 8)^2 C_F^2 + \frac{1}{864}C_F N_f (192\zeta_3 + 1143 - 152\pi^2), \end{aligned} \quad (29)$$

where $\zeta_3 = 1.20206\dots$, $C_F = (N_C^2 - 1)/(2N_C)$, $C_A = N_C$. Using the following relation in the CFG scheme,

$$H_{\alpha,j}^{DY} = 1 + \frac{\alpha_s(Q)}{\pi} H^{DY(1)} + \frac{\alpha_s^2(Q)}{\pi^2} H^{DY(2)} + \dots, \quad (30)$$

⁴Other computer codes are also publicly available at this purpose: DYNNLO [3, 18] and VRAP [2].

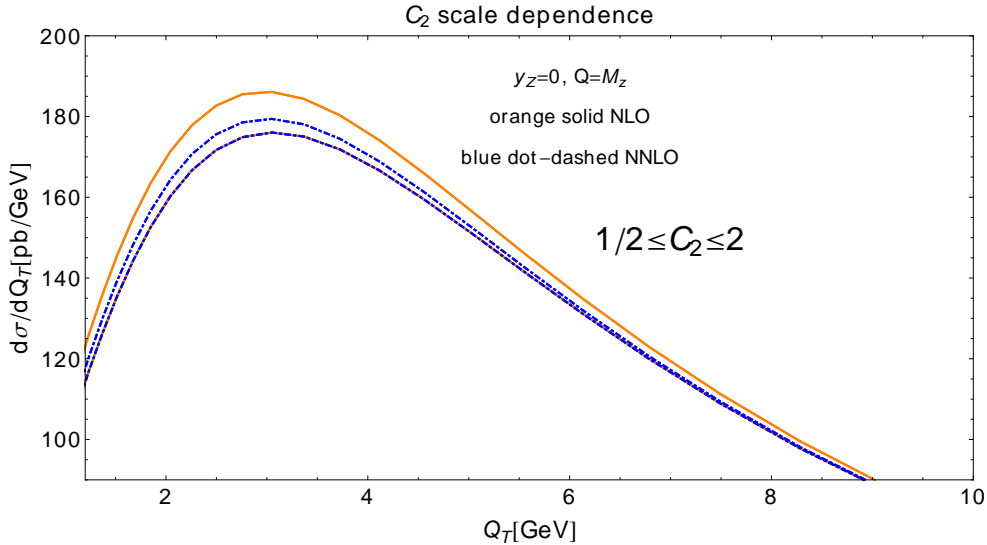


Figure 1: Dependence of Z boson Q_T distribution on the scale parameter C_2 at $\mathcal{O}(\alpha_s^2)$ and $\mathcal{O}(\alpha_s)$.

one can estimate that the impact on H_q^{DY} due to the inclusion of the $\mathcal{O}(\alpha_s^2)$ virtual corrections $H_q^{DY(2)}$ at $Q \approx M_Z$ is about 2%. This correction is of the same order as the magnitude of the effect of about 1% from the averaged coefficient $\langle \delta\mathcal{C}^{(2,c)} \rangle$ in our calculation. This approximation is valid in the kinematic region of W/Z production. The full expression for $\mathcal{C}_{ja}^{(2,c)}(\xi)$ can be implemented in the future numerical work when the experimental errors further decrease.

The effect of the inclusion of scale-dependent terms at $\mathcal{O}(\alpha_s^2)$ is illustrated in Fig. 1 for the Q_T differential cross section for Tevatron Z production at the central rapidity $y_Z = 0$ and $Q = M_Z$. The orange solid band is the $\mathcal{O}(\alpha_s)$ uncertainty obtained by variations of C_2 in the range $0.5 - 2$, while the blue dot-dashed band is the same uncertainty evaluated at $\mathcal{O}(\alpha_s^2)$. The sensitivity of the cross section to C_2 is clearly reduced upon the inclusion of the $\mathcal{O}(\alpha_s^2)$ contribution.

2.5 Nonperturbative resummed contributions

Our fit to the ϕ_η^* will adopt a simple flexible convention [32] for $\widetilde{W}_\alpha(b, Q)$ at $b \gtrsim 1 \text{ GeV}^{-1}$ that can emulate a variety of functional forms arising in detailed nonperturbative models [72, 14, 73, 74, 75, 76, 46, 43, 44].

The convention is motivated by the observation that, given the strong suppression of the deeply nonperturbative large- b region in Z boson production, only contributions from the transition region of b of about 1 GeV^{-1} are non-negligible compared to the perturbative contribution

from $b < 1 \text{ GeV}^{-1}$. In the transition region, $\widetilde{W}(b, Q)$ can be reasonably approximated by the extrapolated leading-power, or perturbative, part $\widetilde{W}^{pert}(b, Q)$, and the nonperturbative smearing factor $\widetilde{W}^{NP}(b, Q)$:

$$\widetilde{W}_{\alpha,j}(b, Q, y_Z) = \widetilde{W}_{\alpha,j}^{pert}(b_*, Q, y_Z) \widetilde{W}^{NP}(b, Q, y_Z). \quad (31)$$

When b is large, the slow b dependence in $\widetilde{W}_{\alpha,j}^{pert}(b_*, Q)$ can be neglected, compared to the rapidly changing $\widetilde{W}_{NP}(b, Q)$. The latter contribution captures the effect of the powerlike contributions proportional to b^p with $p > 0$ that alter the large- b tail of $\widetilde{W}(b, Q)$ in a different way compared to $\widetilde{W}^{pert}(b, Q)$. The powerlike contributions suppress the rate only at Q_T below 2-3 GeV, while the leading-power term and its scale dependence affect a broader interval of Q_T values (see representative figures in Ref. [50]). The nonperturbative suppression results in a characteristic shift of the peak in the $d\sigma/dQ_T$ distribution, which is distinct from the scale dependence.

To avoid divergence due to the Landau pole in $\alpha_s(\bar{\mu})$ at $\bar{\mu} \rightarrow 0$, we redefine the scales of order $1/b$ in $\widetilde{W}^{pert}(b, Q)$ according to the b_* prescription [9, 10] dependent on two parameters [32]. In the Sudakov exponential, the lower limit $(C_1/b)^2$ is replaced by $(C_1/b_*(b, b_{max}))^2$, with

$$b_*(b, b_{max}) \equiv \frac{b}{\sqrt{1 + (b/b_{max})^2}}, \quad (32)$$

where b_{max} is set to 1.5 GeV^{-1} in [32]. To avoid evaluating the PDFs $f_{a/h}(\xi, \mu_F)$ at a factorization scale μ_F below the initial PDF scale $\mu_{ini} \approx 1 \text{ GeV}$, we choose $\mu_F = C_3/b_*(b, C_3/\mu_{ini})$; it is larger than μ_{ini} for any b . This prescription is preferred by the global fit to Drell-Yan Q_T data, where it both preserves the exact perturbative expansion for \widetilde{W}^{pert} at $b < 1 \text{ GeV}^{-1}$ and improves the agreement with the data.

In a broad range of Q values in the Drell-Yan process, the behavior of experimentally observed Q_T distributions is described by [31, 32]

$$\widetilde{W}^{NP}(b, Q) = \exp \left[-b^2 \left(a_1 + a_2 \ln \left(\frac{Q}{2 Q_0} \right) + a_3 \ln \left(\frac{x_1^{(0)} x_2^{(0)}}{0.01} \right) \right) \right], \quad (33)$$

with $x_{1,2}^{(0)} = \frac{Q}{\sqrt{s}} e^{\pm y}$, free parameters a_1, a_2, a_3 , and a fixed dimensional parameter $Q_0 = 1.6 \text{ GeV}$. The b^2 dependence characterizes the leading power-suppressed contribution [72] that can be resolved with the available data. The $\ln(Q)$ dependence is predicted by the Collins-Soper evolution equation [8]. The higher-order power-suppressed contributions proportional to b^4 , etc. cannot be reliably distinguished in the fit from the b^2 term. Although linear contributions proportional to b may also arise from long-distance dynamics [52], they have been empirically disfavored in a global Q_T fit [31].

In the vicinity of Q around M_Z , Eq. (33) reduces to

$$\widetilde{W}^{NP}(b, Q \approx M_Z) = \exp[-b^2 a_Z] \quad (34)$$

with

$$a_Z = a_1 + a_2 \ln\left(\frac{M_Z}{2 Q_0}\right) + a_3 \ln\left(\frac{M_Z^2}{0.01 s}\right). \quad (35)$$

One of the essential applications of CSS resummation formalism concerns the measurement of W boson mass in hadron-hadron collisions. The current most precise W mass measurements obtained by the DØ and CDF collaborations at the Tevatron [77, 78] quote a total error of about 20 MeV, with the bulk of it (approximately 90%) associated with three theoretical sources: PDF uncertainty (of order 10 MeV according to [79]), EW corrections, and the model of $\widetilde{W}_{NP}(b, Q)$ in production of W bosons. The last source of uncertainty appears because the W mass measurements are sensitive to the shape of the cross section in the low- Q_T region.

Once a_Z is determined from Z/γ^* boson production, it is easy to predict \widetilde{W}^{NP} in W boson production at the same \sqrt{s} :

$$\widetilde{W}^{NP}(b, Q \approx M_W) = \exp[-b^2 a_W], \quad (36)$$

where

$$a_W = a_Z + a_2 \ln\left(\frac{M_W}{M_Z}\right) + a_3 \ln\left(\frac{M_W^2}{M_Z^2}\right). \quad (37)$$

For $b_{max} = 1.5 \text{ GeV}^{-1}$, one finds $a_2 = 0.17 \pm 0.03 \text{ GeV}^2$ and $a_3 = -0.03 \pm 0.02 \text{ GeV}^2$ [32], where the error estimate includes the scale dependence. The log terms proportional to a_2 and a_3 are small in Eq. (37), so that it is safe to assume $a_W \approx a_Z$ in central-rapidity measurements at the same \sqrt{s} .

If Q is substantially different from M_Z , or if predictions for the LHC are made, the a_2 and a_3 contributions cannot be neglected. The nonperturbative coefficient becomes

$$a(Q, \sqrt{s}) = a_Z(1.96 \text{ TeV}) + a_2 \ln\left(\frac{Q}{M_Z}\right) + a_3 \ln\left(\frac{Q^2}{M_Z^2} \frac{s}{(1.96 \text{ TeV})^2}\right). \quad (38)$$

2.6 Matching the W and Y terms

By examining the mapping of Q_T distributions on ϕ_η^* distributions discussed in Sec. 2.1, we can identify three regions with distinct QCD dynamics: the resummation region $\phi_\eta^* \lesssim 0.1$ rad, where the W term dominates; the intermediate (matching) region $0.1 \lesssim \phi_\eta^* \lesssim 0.5$ rad; and the perturbative region $\phi_\eta^* \gtrsim 0.5$ rad, where the $W + Y$ term approaches the fixed-order (FO) contribution. As ϕ_η^* increases in the intermediate region, the $W + Y$ term eventually becomes

smaller than the FO term at $\phi_\eta^* \equiv \phi_{switch}(Q, y_Z)$. The final cross section is taken to be equal to the $W + Y$ term at $\phi_\eta^* < \phi_{switch}$ and FO term at $\phi_\eta^* \geq \phi_{switch}$ [30].

The position of the switching point is subject to some variations dependent on the shapes of the W term and its asymptotic expansion at not too small $\phi_\eta^* \propto Q_T/Q$, *i.e.* away from the $Q_T^2/Q^2 \rightarrow 0$ limit where the W term is uniquely defined. These variations have almost no effect on the fit of the nonperturbative function in the resummation region ϕ_η^* . They originate from the possibility of including additional terms of order Q_T^2/Q^2 in the longitudinal momentum fractions $\chi_{1,2}$ in the W term and its asymptotic expansion. These terms vanish at $Q_T^2/Q^2 \rightarrow 0$, but they can be numerically important or even desirable in the intermediate region, where they may improve agreement between the $W + Y$ and FO terms.

At intermediate Q_T/Q , radiation of a Z boson and semi-hard jets requires sufficient center-of-mass energy of incident partons, or large enough partonic momentum fractions ξ_1 and ξ_2 . For example, the FO hadronic cross section is written as

$$\begin{aligned} \frac{d\sigma}{dQ^2 dy_Z dQ_T^2} &= \sum_{a,b} \int_0^1 d\xi_1 \int_0^1 d\xi_2 \frac{d\hat{\sigma}}{dQ^2 dy_Z dQ_T^2} f_{a/A}(\xi_1) f_{b/B}(\xi_2) \\ &\equiv \int_{\bar{\xi}_1}^1 d\xi_1 \int_{\bar{\xi}_2}^1 d\xi_2 h(\xi_1, \xi_2) \delta \left[\left(\frac{\xi_1}{x_1} - 1 \right) \left(\frac{\xi_2}{x_2} - 1 \right) - \frac{Q_T^2}{M_T^2} \right], \end{aligned} \quad (39)$$

where $h(\xi_1, \xi_2)$ contains the hard-scattering matrix element and PDFs, and $M_T = \sqrt{Q^2 + Q_T^2}$. The energy constraint from the δ -function imposes the following boundaries on the partonic momentum fractions: $\xi_1 = x_1 + (Q_T^2/s)/(\xi_2 - x_2)$; $\bar{\xi}_1 = [x_1 + (Q_T^2/s)/(1 - x_2)] \leq \xi_1 \leq 1$; $\bar{\xi}_2 \equiv [x_2 + (Q_T^2/s)/(1 - x_1)] \leq \xi_2 \leq 1$, with $x_{1,2} = \frac{M_T}{\sqrt{s}} e^{\pm y}$.

These boundaries are absent in the W and asymptotic contributions, which depend on convolutions of Wilson coefficient functions and PDFs,

$$[C_{j,a} \otimes f_{a/h_i}] (\chi_i, \mu_F) = \int_{\chi_i}^1 \frac{d\xi_i}{\xi_i} C_{j,a} \left(\frac{\chi_i}{\xi_i}, \mu_{Fb}, C_1, C_2, C_3 \right) f_{a/h_i}(\xi_i, \mu_F) \quad (40)$$

for $i = 1$ or 2 . The variables χ_i satisfy $\chi_{1,2} \rightarrow x_{1,2}^{(0)} \equiv (Q/\sqrt{s})e^{\pm y}$ and cannot exceed $\bar{\xi}_{1,2}$. Thus, for non-negligible Q_T^2/Q^2 , the W and asymptotic term may include contributions from the unphysical momentum fractions $\xi_i \leq \bar{\xi}_i$, and ideally one should include kinematically important Q_T^2/Q^2 contributions into $\chi_{1,2}$ to bring them as close to $\bar{\xi}_{1,2}$ as possible.

As the procedure for including the Q_T^2/Q^2 corrections in the W term is not unique, we explored several of them. We find that either $\chi_{1,2} = x_{1,2}^{(0)} = (Q/\sqrt{s})e^{\pm y}$ or $\chi_{1,2} = x_{1,2} = (M_T/\sqrt{s})e^{\pm y}$ results in the comparable agreement with the ϕ_η^* data from DØ and ATLAS 7 TeV. These prescriptions are designated as the “kinematical corrections of type 0” and “type 1”, or kc_0 and kc_1 , in our numerical outputs.

In contrast, some alternative choices produce worse agreement with the examined data, such as $\chi_{1,2} = \bar{\xi}_{1,2} = ((M_T + Q_T)/\sqrt{s})e^{\pm y}$ designated as kc_2 . Furthermore, the kc_1 prescription improves matching compared to kc_0 at $\sqrt{s} = 14$ TeV, corresponding to scattering at smaller x . We use the kc_1 matching as the default prescription in the subsequent comparisons.

Dependence on the matching prescription at intermediate Q_T (intermediate ϕ_η^*) reflects residual sensitivity to higher-order contributions and is reduced [30] once large- Q_T contributions of $\mathcal{O}(\alpha_s^2)$ are included, compared to $\mathcal{O}(\alpha_s)$. The RESBOS implementation follows a general argument for matching of the resummed contribution onto the fixed-order result that applies in other areas, such as the treatment of PDFs for heavy quarks in DIS in a general-mass variable number scheme [80, 81]. Matching is stabilized by constructing resummed coefficient functions that comply with the energy-momentum conservation in the exact fixed-order contribution.

2.7 Photon radiative contributions

Our resummed calculations include both Z -mediated and photon-mediated contributions to production of Drell-Yan pairs, as well as their interference. Electroweak radiative contributions have been extensively studied in Z boson [83, 84, 85, 86] and W boson production [87, 88, 89, 90, 91, 92]. The dominant NLO electroweak contribution is associated with final-state radiation of photons. To compare the $D\bar{O}$ data to the RESBOS prediction without the NLO electroweak correction, we correct the fitted data to the Born level for final-state leptons by subtracting the NLO EM correction obtained bin-by-bin by the PHOTOS code [93]. This correction is essential for the agreement of RESBOS theory and data. However, since the photon-mediated and final-state photon radiation contributions are relatively small, in the first approximation we can treat them as a linear perturbation and evaluate for a fixed combination of the nonperturbative and scale parameters taken either from the BLNY or our best-fit parametrizations.

2.8 Numerical accuracy

Given the complexity of the resummation calculation, we expect several sources of random numerical errors that may compete with the accuracy of the most precise ϕ_η^* data points, which are of order 0.5% of the respective central cross sections. The numerical errors may arise from the parametrizations of PDFs, integration, and interpolation at various stages of the analysis. They can be treated as independent and uncorrelated and primarily result in higher-than-normal values of the figure-of-merit function χ^2 when not explicitly included in the estimates. In comparison, the variations due to a_Z or $C_{1,2,3}$ parameters are of order a few percent and correlated across the ϕ_η^* spectrum.

2.9 A comparison with an alternative formalism

In the last part of this section, it is instructive to summarize the distinctions between the NNLL/NNLO resummed Q_T distributions obtained in the CSS formalism and the alternative approach of Refs. [82, 19, 28]. Both methods predict Q_T distributions in a wide range of processes, including production of lepton pairs and Higgs boson. While sharing the same physics principles, they organize the small- Q_T form factor W in distinct ways and differ in the form of their higher-order corrections and quantitative dependence on QCD scales.

We will outline the key differences by referring to the work by Bozzi, Catani, de Florian, and Grazzini (BCFG) in Ref. [82]. There, the BCFG representation was derived step-by-step and compared to the CSS method in the kin process of $gg \rightarrow$ Higgs production. The general observations of that paper also apply to the Drell-Yan process.

In both formalisms, the resummed Q_T distribution for $h_1 h_2 \rightarrow VX$, where $V = \gamma^*, Z$, and upon integration over the decay angles of the lepton pair, is constructed from the small- Q_T resummed, large- Q_T fixed-order, and asymptotic (overlap) contributions, denoted as W , FO, and $(W)_{\text{FO}}$:

$$\frac{d\sigma(h_1 h_2 \rightarrow VX)}{dQ^2 dy_Z dQ_T^2} = W + \text{FO} - (W)_{\text{FO}} = W + Y. \quad (41)$$

In accord with the preceding discussion, the W term of the CSS formalism takes form, in a simplified notation, of

$$W(Q, Q_T, y_Z) = \int \frac{bdb}{4\pi} J_0(Q_T b) \widetilde{W}_{\text{CSS}}(b, Q, y_Z). \quad (42)$$

The integrand consists of the zeroth order Bessel function, $J_0(Q_T b)$, and the form factor $\widetilde{W}_{\text{CSS}}$ that is derived in the context of TMD factorization. At $b \ll 1 \text{ GeV}^{-1}$, the form factor is expressed as

$$\begin{aligned} \widetilde{W}_{\text{CSS}}(b, Q, y_Z) &= \sum_{j,a,b} \int_0^1 d\xi_1 \int_0^1 d\xi_2 f_{a/h_1}(\xi_1, \mu_F) f_{b/h_2}(\xi_2, \mu_F) \\ &\times |H_j(Q, \mu_Q/Q; \alpha_S(\mu_Q))|^2 \exp \left[- \int_{\mu_b}^{\mu_Q} \frac{d\mu^2}{\mu^2} A(\alpha_S(\mu), \mu_b b) \ln \left(\frac{\mu_Q^2}{\mu^2} \right) + B(\alpha_S(\mu), \mu_b b, \mu_Q/Q) \right] \\ &\times C_{ja} \left(\frac{\chi_1}{\xi_1}, \frac{\mu_Q}{\mu_b}, \mu_F b \right) C_{jb} \left(\frac{\chi_2}{\xi_2}, \frac{\mu_Q}{\mu_b}, \mu_F b \right). \end{aligned} \quad (43)$$

$\widetilde{W}_{\text{CSS}}$ depends on three QCD scales: $\mu_b = C_1/b$, $\mu_Q = C_2 Q$, $\mu_F = C_3/b$, where the arbitrary scale constants C_1 , C_2 , and C_3 are of order unity. Their exact values are chosen so as to optimize the convergence of the perturbative series. The combination $C_1 = C_3 = b_0$, $C_2 = 1$ is the natural choice.

In Ref. [82, 19], the resummed form factor \widetilde{W}_{BCFG} in the second approach is written at $b \ll 1 \text{ GeV}^{-1}$ as

$$\begin{aligned} \widetilde{W}_{BCFG}(b, Q, y_Z) = \\ \sum_{j,a,b} \int_0^1 d\xi_1 \int_0^1 d\xi_2 f_{a/h_1}(\xi_1, \bar{\mu}_F) f_{b/h_2}(\xi_2, \bar{\mu}_F) W_{j,ab}(b, Q, \xi_1 \xi_2 s; \bar{\alpha}_s, \bar{\mu}_R, \bar{\mu}_F). \end{aligned} \quad (44)$$

$W_{j,ab}$ is reconstructed from its N -th Mellin moments $W_{ab,N}$ that are expanded in powers of $\alpha_s(\bar{\mu}_R) \equiv \bar{\alpha}_s$. $W_{ab,N}$ consists of the function $\mathcal{H}_{j,ab,N}$ that depends only on scales of order Q , and the exponent $e^{\mathcal{G}_N}$ that depends on $\tilde{L} \equiv \ln(Q^2 b^2 / b_0^2 + 1)$ and ratios of various scales:

$$\begin{aligned} W_{ab,N}(b, Q; \bar{\alpha}_s, \bar{\mu}_R, \bar{\mu}_F) = \\ \mathcal{H}_{j,ab,N}(Q, \bar{\alpha}_s, Q/\bar{\mu}_R, Q/\bar{\mu}_F, Q/\bar{\mu}_Q) \cdot \exp \left\{ \mathcal{G}_N \left(\bar{\alpha}_s, \tilde{L}; Q/\bar{\mu}_R, Q/\bar{\mu}_Q \right) \right\}. \end{aligned} \quad (45)$$

On the right-hand side, the representation includes three auxiliary QCD scales, each taken to be of order of the boson's virtuality Q : the resummation scale $\bar{\mu}_Q$, the renormalization scale $\bar{\mu}_R$, and the PDF factorization scale $\bar{\mu}_F$. The dependence on b enters only through the logarithmic term \tilde{L} inside $e^{\mathcal{G}_N}$.

The representation $\widetilde{W}_{BCFG}(b, Q, y_Z)$ in Eqs. (44, 45) can be obtained from $\widetilde{W}_{CSS}(b, Q, y_Z)$ in Eq. (43) by a series of steps that are documented in [82].

First, the QCD scales are selected differently in the two approaches. In $\widetilde{W}_{CSS}(b, Q, y_Z)$ several terms depend on the variable scales $\mu_b = C_1/b$ and $\mu_F = C_3/b$. The QCD scale $C_2 Q$ plays the role that is similar to the resummation scale $\bar{\mu}_Q$. Inside the Sudakov integral, the scale μ in $\alpha_s(\mu)$ is integrated over.

In $\widetilde{W}_{BCFG}(b, Q, y_Z)$, the scales $\bar{\mu}_b$ and $\bar{\mu}_F$ are fixed at b_0/b . The QCD coupling strength $\alpha_s(\mu)$ is converted into the series of $\bar{\alpha}_s$ (at the scale $\bar{\mu}_R \sim Q$) using the renormalization group equations. The collinear PDFs $f_{a/h}(\xi, \mu)$ in Eqs. (43) and (44) are evaluated at $\mu_F \sim 1/b$ in $\widetilde{W}_{CSS}(b, Q, y_Z)$, and $\bar{\mu}_F \sim Q$ in $\widetilde{W}_{BCFG}(b, Q, y_Z)$. To preserve the factorization scale invariance, the Mellin moment $W_{ab,N}$ of the BCFG form factor explicitly includes an operator matrix $\mathbf{U}_N(b_0/b, \bar{\mu}_F)$ for DGLAP evolution of $f_{a/h}(\xi, \mu)$ between the scales $\bar{\mu}_F$ and b_0/b , while the CSS form factor does not.⁵

After the conversion $\alpha_s(\mu) \rightarrow \bar{\alpha}_s$ in $W_{ab,N}$, the contributions at scales of order Q are included into $\mathcal{H}_{j,ab,N}$ as in Eq. (45). The Sudakov integral $S(b, Q; C_1, C_2) = S(\mu_Q/\mu_b)$ and the anomalous

⁵More specifically, $W_{ab,N}$ in Appendix A of [82] includes the evolution operator that is factorized as $\mathbf{U}_N(b_0/b, \bar{\mu}_F) = \mathbf{U}_N(b_0/b, \bar{\mu}_Q) \mathbf{U}_N(\bar{\mu}_Q, \bar{\mu}_F)$. $\mathbf{U}_N(b_0/b, \bar{\mu}_Q)$ is exponentiated inside \mathcal{G}_N . $\mathbf{U}_N(\bar{\mu}_Q, \bar{\mu}_F)$ is retained in $\mathcal{H}_{j,ab,N}$.

dimensions of various components are assimilated into \mathcal{G}_N . Within \mathcal{G}_N , all evolution operators are expanded as a series in $\bar{\alpha}_s$ and $L = \ln(Q^2 b^2/b_0^2)$:

$$\mathcal{G}_N = Lg^{(1)}(\bar{\alpha}_s L) + g^{(2)}\left(\bar{\alpha}_s L; \frac{Q}{\bar{\mu}_R}, \frac{Q}{\bar{\mu}_Q}\right) + \frac{\bar{\alpha}_s}{\pi} g^{(3)}\left(\bar{\alpha}_s L; \frac{Q}{\bar{\mu}_R}, \frac{Q}{\bar{\mu}_Q}\right) + \dots \quad (46)$$

Finally, a prescription for matching of the $W + Y$ and FO terms at large Q_T is introduced in \widetilde{W}_{BCFG} by replacing all generic logarithms $L = \ln(Q^2 b^2/b_0^2)$ in $e^{\mathcal{G}_N}$ by $\tilde{L} = \ln(Q^2 b^2/b_0^2 + 1)$. The replacement forces the exponential to satisfy $e^{\mathcal{G}_N} \rightarrow 1$ when $b_0^2/b^2 \ll Q^2$, i.e., in the region of the small transverse positions b that dominate the Fourier-Bessel integral when Q_T is large. The resulting outcome is that the W and asymptotic terms cancel well at large Q_T , and that, upon the integration over Q_T , the inclusive $W + Y$ cross section turns out to be exactly equal to the fixed-order cross section. In the BCFG cross section, matching therefore arises as a result of a mathematical replacement $L \rightarrow \tilde{L}$ in the resummed exponential, and not because of the physical constraint due to energy-momentum conservation imposed in our approach. The $L \rightarrow \tilde{L}$ matching works by suppressing the \mathcal{G}_N exponent at $b^2 \ll 1/Q^2$ via a deft, even though not unique, redefinition of L (see also Ref. [94]).

In the CSS approach adopted in RESBOS, the scale constants C_1 and C_3 need not to equal b_0 exactly. The Sudakov integral $S(\mu_Q/\mu_b)$ is evaluated numerically and not as a logarithmic expansion in powers of L as it is done in $\widetilde{W}_{BCFG}(b, Q, y_Z)$. The RESBOS code does not operate with the independent QCD scales $\bar{\mu}_R \sim Q$ and $\bar{\mu}_F \sim Q$ of the BCFG formalism.

RESBOS finds $\alpha_s(\mu)$ by numerically solving the renormalization group equation and always evolves the PDFs $f_{a/h}(\xi, \mu_F)$ forward from the initial scale $Q_0 \approx 1$ GeV of the input PDF ensemble to a higher scale $\mu_F \geq Q_0$. This is to be contrasted with $\widetilde{W}_{BCFG}(b, Q, y_Z)$, which implements the logarithmic expansion for $\alpha_s(\mu)$ and the DGLAP matrix operator $\mathbf{U}_N(b_0/b, \bar{\mu}_Q)$ that evolves the PDFs $f_{a/h}(\xi, \bar{\mu}_F)$ backward from $\bar{\mu}_Q \approx Q$ down to a lower scale b_0/b in the most relevant b region. The backward evolution of this kind has a tendency to be unstable and cause the PDFs to deviate at low momentum scales. Hence the numerical evolution of $\alpha_s(\mu)$ and forward DGLAP evolution adopted in $\widetilde{W}_{CSS}(b, Q, y_Z)$ is more trustworthy in precision studies.

The nonperturbative contribution arises in $\widetilde{W}_{CSS}(b, Q, y_Z)$ as a natural feature of QCD factorization in terms of TMD PDFs. Dependence on matching is present, implicitly or explicitly, in either formalism. When looking for evidence of nonperturbative effects in ϕ_η^* distributions, it is desirable to investigate several prescriptions for matching of low- Q_T and high- Q_T terms. We have done it by varying the form of the rescaling variables that control the cross sections in the matching region in RESBOS.

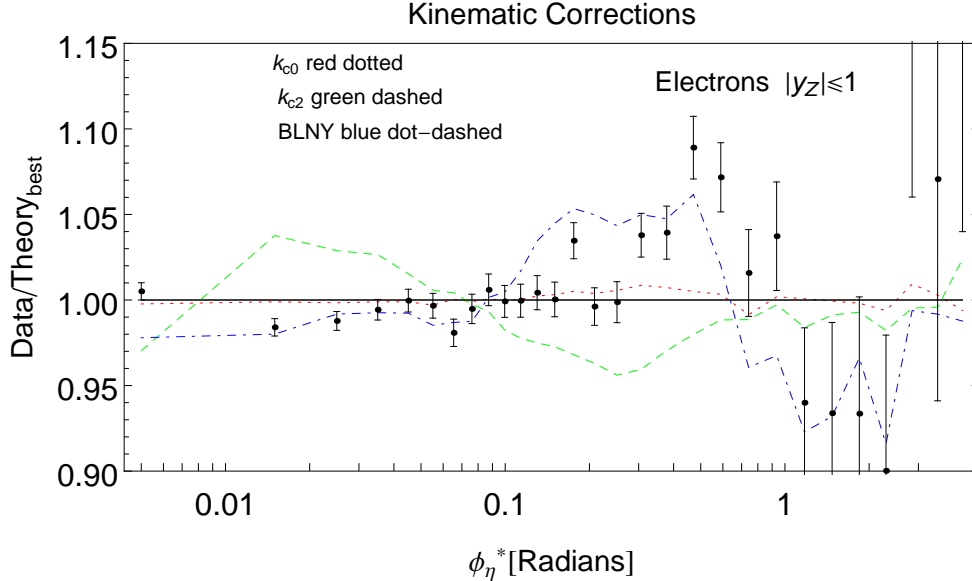


Figure 2: The ratios to the central theoretical prediction of the DØ electron data at $|y_Z| \leq 1$ and alternative theoretical predictions. The central prediction is computed assuming $C_1 = C_3 = 2b_0$, $C_2 = 1/2$, $a_Z = 1.1 \text{ GeV}^2$, and kinematical correction 1. Theory predictions based on alternative kinematical corrections (0 and 2) and BLNY nonperturbative parametrization are also shown.

3 Numerical results

3.1 General features

In this section we determine a_Z from the distribution $(1/\sigma) d\sigma/d\phi_\eta^*$ measured by DØ [25] that is normalized to the total cross section σ in the measured Q and y range. These data are given in three bins of Z boson rapidity y_Z . In the first two, $|y_Z| \leq 1$ and $1 \leq |y_Z| \leq 2$, the $(1/\sigma) d\sigma/d\phi_\eta^*$ distribution is measured separately for electrons and muons at $N_{pt} = 29$ points of ϕ_η^* . In the third bin, $|y_Z| \geq 2$, only electrons are measured at 25 points of ϕ_η^* . The first two y_Z bins provide substantial new constraints. The third bin has larger statistical errors and reduced discriminating power.

All predictions are obtained by using CT10 NNLO PDFs [54]. Predictions based on MSTW'08 NNLO PDF sets [95] were also computed and did not show significant difference with CT10 NNLO predictions.

From the previous section, the resummed cross sections depend on the perturbative scales, power-suppressed contributions, and choice of subleading kinematic terms. It is possible to

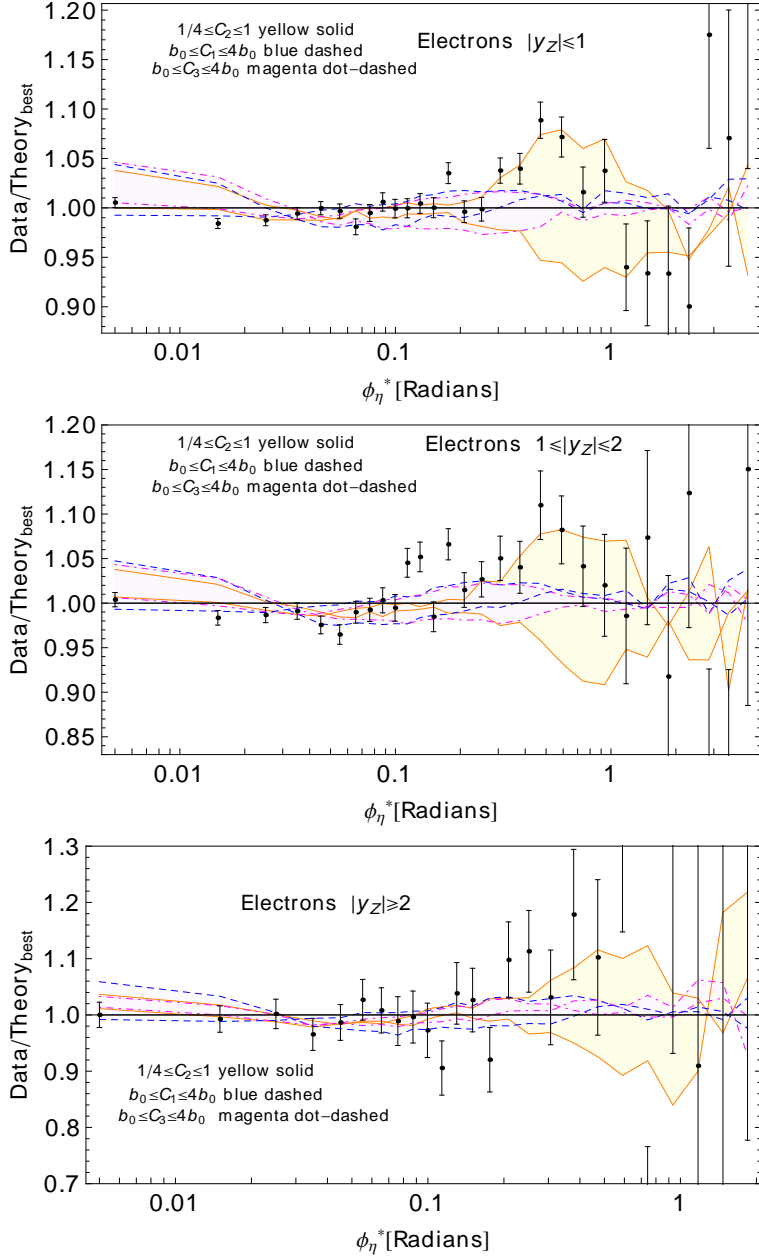


Figure 3: Electrons: scale variation due to $C_{1,2,3}$ at small ϕ_η^* .

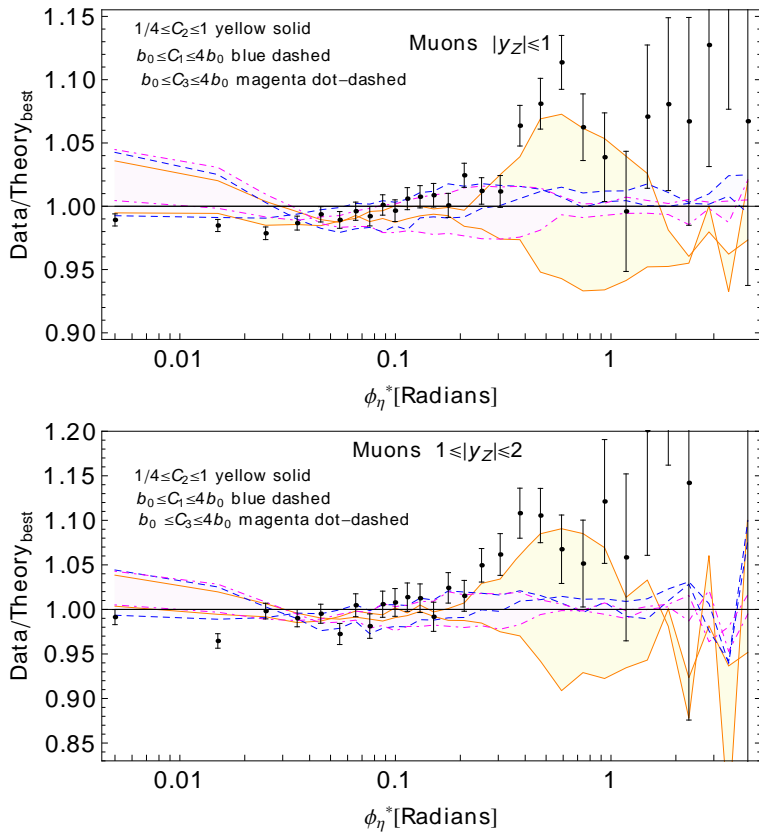


Figure 4: Same as above but for the muons.

identify an optimal combination of these factors that results in a good description of the $D\bar{O}$ data across the full ϕ_η^* range. In particular, the large- Q_T /large- ϕ_η^* data generally prefer the factorization scale of order $Q/2$ or even less in the fixed-order piece. At small- Q_T (small- ϕ_η^*), the scale parameter C_3 in the range $1.5b_0 - 2b_0$ is slightly more preferable. To illustrate properties of the ϕ_η^* distributions, we compute the resummed cross sections using a combination $C_1 = C_3 = 2 b_0$, $C_2 = Q/2$, and $a_Z = 1.1 \text{ GeV}^2$ that is close to the best-fit solution. The difference between the best-fit solution and the prediction based on these round-off values will be discussed in Sec. 3.2.

A comparison of the prediction with these choices to the $D\bar{O}$ data for $|y_Z| \leq 1$ and a few other predictions is presented in Fig. 2. The new parametrization provides better description of the data at $0.1 \leq \phi_\eta^* \leq 1$ than the superimposed prediction utilizing the BLNY parametrization [31] of \widetilde{W}^{NP} . Consequently, it results in a better χ^2 than the RESBOS prediction used in the $D\bar{O}$ analysis [25], which used the CTEQ6.6 NLO PDFs, BLNY \widetilde{W}_{NP} , and canonical choice of $C_{1,2,3}$.

We also compare predictions for three types (0, 1, 2) of the kinematical (matching) correction discussed in Sec. 2.6. For the selected combination of scale parameters, the type-0 and 1 kinematical corrections provide a nearly identical prediction. The type-0 and type-1 corrections can differ by 2-3% for other scales. Type 2 is generally disfavored, so that we assume the type-1 correction for the rest of the analysis.

A prediction with the same theoretical parameters, as well as for variations in QCD scales in the ranges $1/4 \leq C_2 \leq 1$ and $b_0 \leq C_{1,3} \leq 4b_0$, are compared to the data for electron production in Fig. 3 and muon production in Fig. 4. Here we show all rapidity bins both for electron and muon samples. The ratios of the $D\bar{O}$ data to RESBOS theory with the optimal parameters are indicated by black circles. Yellow solid, blue dashed, and magenta dot-dashed bands represent variations in theory due to C_2 , C_1 , and C_3 , respectively, all normalized to the best-fit prediction. Again, the agreement with RESBOS observed in these figures is better than in [25]. Figs. 3 and 4 demonstrate that the theoretical uncertainty at small ϕ_η^* is dominated by variations of C_1 and C_3 . The bands of scale uncertainty are reduced significantly for $0.04 \leq \phi_\eta^* \leq 0.1$ upon the inclusion of $\mathcal{O}(\alpha_s^2)$ scale dependence, as has been discussed in Sec. 2.4.

The scale variations can be compared to the dependence on a_Z and kinematic correction in Fig. 5, which result in distinctly different patterns of variation in $d\sigma/d\phi_\eta^*$. In particular, while the perturbative scale coefficients C_1, C_2, C_3 produce a slowly changing variation across most of the measured ϕ_η^* range, the increase in a_Z produces a distinct variation that suppresses the rate at $\phi_\eta^* \lesssim 0.02$ and increases it at $0.02 \lesssim \phi_\eta^* \lesssim 0.5$, with the rate above 0.5 essentially unaffected. A similar behavior was observed in Fig. 6 of [50] with a different NP function and a different

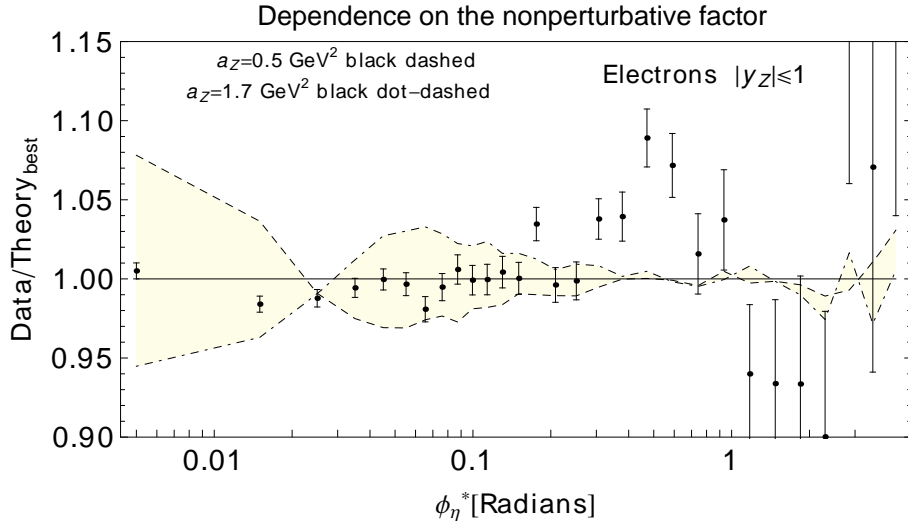


Figure 5: Dependence on the nonperturbative parameter a_Z for electrons with $|y_Z| \leq 1$.

procedure that varied all QCD scales around the central values of order of the dilepton's mass.

It is therefore possible to separate the scale dependence from the a_Z dependence if we restrict the attention to ϕ_η^* below and around $\phi_\eta^* = 0.1$. To this aim we consider only the first 12 bins of ϕ_η^* , starting from the smallest value, for each value of rapidity. Extending the fitted range above $\phi_\eta^* \geq 0.1$ has a minimal effect on a_Z .

3.2 Detailed analysis

We pursue two approaches for the examination of the low- ϕ_η^* region. In method I, we study the dependence on a_Z by assuming fixed resummation scales corresponding to half-integer scale parameters, such as $C_1/b_0 = C_3/b_0 = 1, C_2 = 1/2$ or $C_1/b_0 = C_3/b_0 = 2, C_2 = 1/2$. In this method, the goodness-of-fit function χ^2 is minimized with respect to a_Z for select combinations of fixed scale parameters. We find that a χ^2 minimum with respect to a_Z exists in these cases, but, given the outstanding precision of the ϕ_η^* data, the best-fit χ^2/N_{pt} remains relatively high, of order 2-3. This is partly due to the numerical noise discussed in Sec.2.8.

The χ^2 function can be further reduced by allowing arbitrary $C_{1,2,3}$ parameters, in particular, by taking C_2 to be *below* $1/2$. In this context, one has to decide on the acceptable range of variations in $C_{1,2,3}$, *i.e.* the resummation scales.

As computations for multiple combinations of a_Z and $C_{1,2,3}$ parameters would be prohibitively CPU-extensive, in method II we first consider a fixed scale combination indicated by $\{\bar{C}_1, \bar{C}_2, \bar{C}_3\}$ and implement a linearized model for small deviations of the scale parameters

from $\bar{C}_{1,2,3}$. The central combination $\bar{C}_{1,2,3}$, namely $\bar{C}_1 = \bar{C}_3 = 2b_0$, $\bar{C}_2 = 1/2$, produces good agreement with the data, although not as good as completely free $C_{1,2,3}$. The linearized model is explained in Sec. 3.2.2. It provides a fast estimate of small correlated changes in the ϕ_η^* shape of the kind shown in Figs. 3 and 4.

The χ^2 function is sampled at discrete a_Z values in the interval $a_Z = [0.1 : 3.5]$ GeV² and reconstructed between the sampling nodes by using polynomial interpolation. When the scale variations are allowed, the dependence of χ^2 on a_Z is asymmetric and very different from a quadratic one.

To account for the asymmetry of the distributions, we quote the central value \bar{a}_Z that minimizes $\chi^2(a_Z)$ and the 68% confidence level (C.L.) uncertainty. The probability density function $\mathcal{P}(a_Z)$ for a_Z in a sample with N points is taken to follow a chi-squared distribution with N degrees of freedom,

$$\mathcal{P}(a_Z) = \mathcal{P}_\chi(N, \chi^2(a_Z)) = \frac{(\chi^2)^{N/2-1} \exp(-\chi^2/2)}{\Gamma(N/2) 2^{N/2}}. \quad (47)$$

With this, we determine the 68% C.L. intervals $[a_{Z,min}, a_{Z,max}]$, where $a_{Z,min}$ and $a_{Z,max}$ are defined implicitly by

$$0.16 = \frac{\int_0^{a_{Z,min}} \mathcal{P}(a_Z) da_Z}{\int_0^{+\infty} \mathcal{P}(a_Z) da_Z}, \quad 0.84 = \frac{\int_0^{a_{Z,max}} \mathcal{P}(a_Z) da_Z}{\int_0^{+\infty} \mathcal{P}(a_Z) da_Z}. \quad (48)$$

For an asymmetric distribution as in method II, the central value \bar{a}_Z does not coincide with the middle of the 68% C.L. interval or the mean a_Z given by the first moment of the $\mathcal{P}(a_Z)$ distribution.

3.2.1 Method I: minimization with fixed scale parameters

In method I, a_Z is determined from the DØ data by minimization of a function

$$\chi^2(a_Z) = \sum_{i=1}^{N_{pt}} \left(\frac{D_i - \bar{T}_i(a_Z)}{s_i} \right)^2, \quad (49)$$

where D_i are the data points; $\bar{T}_i(a_Z)$ are the theoretical predictions for fixed scale parameters $\{\bar{C}_1, \bar{C}_2, \bar{C}_3\}$; s_i are the uncorrelated experimental uncertainties; and N_{pt} is the number of points.

The dependence of χ^2 on a_Z in three rapidity bins for two combinations of $\bar{C}_{1,2,3}$ is illustrated in Fig. 6, and the corresponding best-fit parameters are listed in Table 1. Electrons and muons are combined in the first two bins of rapidity, $|y_Z| \leq 1$ and $1 \leq |y_Z| \leq 2$. In both cases, the χ^2 behavior is close to parabolic. The locations of the χ^2 minima are consistent in all three bins. However, the quality of the fit is unacceptable in the first two bins that have the

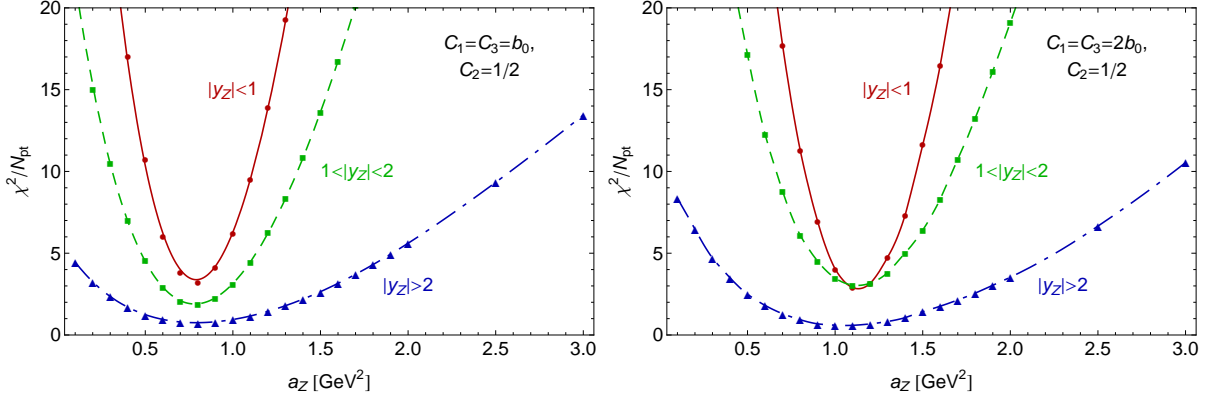


Figure 6: χ^2/N_{pt} as a function of a_Z with fixed $C_{1,2,3}$.

smallest experimental errors, with $\chi^2/N_{pt} \approx 3$. On the other hand, the agreement is very good ($\chi^2/N_{pt} < 1$) in the third bin, which has larger errors.

The weighted averages over all three bins are $\bar{a}_{Z,\text{all } y} = 0.79 \pm 0.03$ and 1.12 ± 0.07 GeV² for the two scale combinations. The location of the minimum is distinct from zero in both cases, but its dependence on the scale parameters warrants further investigation that we will now perform.

3.2.2 Method II: computation with scale-parameter shifts

To simplify the minimization when the scale parameters are varied, we introduce a linearized approximation for the covariance matrix of the type adopted for evaluating correlated systematic effects in PDF fits [96, 97]. For each scale parameter C_α , $\alpha = 1, 2, 3$, we define a nuisance parameter $\lambda_\alpha \equiv \log_2(C_\alpha/\bar{C}_\alpha)$ and compute the finite-difference derivatives of theory cross sections

$$\beta_{i\alpha} \equiv \frac{T_i(a_Z, \lambda_\alpha = +1) - T_i(a_Z, \lambda_\alpha = -1)}{2}, \quad \alpha = 1, 2, 3; \quad i = 1, \dots, N_{pt} \quad (50)$$

over the interval $\lambda_\alpha = \pm 1$ corresponding to $\bar{C}_\alpha/2 \leq C_\alpha \leq 2\bar{C}_\alpha$. Variations of λ_α introduce correlated shifts in theory cross sections $T_i(a_Z, C_{1,2,3})$ with respect to the fixed-scale theory cross sections $T_i(a_Z, \bar{C}_{1,2,3}) \equiv \bar{T}_i(a_Z)$. We can reasonably assume that the probability distribution over each λ_α is similar to a Gaussian one with a central value of 0 and half-width σ_λ , taken to be the same for all λ_α . The goodness-of-fit function is then defined as

$$\chi^2(a_Z, \lambda_{1,2,3}) = \sum_{i=1}^{N_{pt}} \left(\frac{D_i - \bar{T}_i(a_Z) - \sum_{\alpha=1}^3 \beta_{\alpha i} \lambda_\alpha}{s_i} \right)^2 + \sum_{\alpha=1}^3 \frac{\lambda_\alpha^2}{\sigma_\lambda^2}. \quad (51)$$

Fit results for $\phi_\eta^* \leq 0.1$			
	N_{pt}	χ_{min}^2/N_{pt}	$\bar{a}_Z \pm \delta a_Z$ (GeV ²)
$ y_Z \leq 1, \quad e + \mu$	24	3.24	$0.79^{+0.2}_{-0.03}$
		2.83	1.14 ± 0.08
$1 \leq y_Z \leq 2, \quad e + \mu$	24	1.87	0.79 ± 0.05
		3.03	$1.12^{+0.14}_{-0.13}$
$ y_Z \geq 2, \quad e$	12	0.74	$0.8^{+0.03}_{-0.05}$
		0.58	$1.04^{+0.18}_{-0.16}$
All y_Z bins, weighted average	60	2.19	0.79 ± 0.03
		2.46	1.12 ± 0.07

Table 1: The best-fit χ^2/N_{pt} , central value and 68% C.L. intervals for a_Z with fixed $C_{1,2,3} = \{b_0, 1/2, b_0\}$ (upper lines) and $\{2b_0, 1/2, 2b_0\}$ (lower lines).

The minimum with respect to λ_α can be found algebraically for every a_Z as [96]

$$\min \chi^2 = \chi^2(a_Z, \bar{\lambda}_\alpha) = \sum_{i,j}^{N_{pt}} (D_i - \bar{T}_i(a_Z)) (\text{cov}^{-1})_{ij} (D_j - \bar{T}_j(a_Z)), \quad (52)$$

containing the inverse of the covariance matrix,

$$(\text{cov}^{-1})_{ij} = \left[\frac{\delta_{ij}}{s_i^2} - \sum_{\alpha,\beta=1}^3 \frac{\beta_{i,\alpha}}{s_i^2} \mathcal{A}_{\alpha\beta}^{-1} \frac{\beta_{j,\beta}}{s_j^2} \right], \quad (53)$$

and a matrix \mathcal{A} given by

$$\mathcal{A}_{\alpha\beta} = \sigma_\lambda^2 \delta_{\alpha\beta} + \sum_{k=1}^{N_{pt}} \frac{\beta_{k,\alpha} \beta_{k,\beta}}{s_k^2}. \quad (54)$$

Eq. (52) is essentially the standard χ^2 function based on the covariance matrix in the presence of the correlated shifts. For every a_Z , the nuisance parameters $\bar{\lambda}_\alpha$ that realize the χ^2 minimum are also known,

$$\bar{\lambda}_\alpha(a_Z) = \sum_{i=1}^{N_{pt}} \frac{D_i - \bar{T}_i(a_Z)}{s_i} \sum_{\delta=1}^3 \mathcal{A}_{\alpha\delta}^{-1} \frac{\beta_{i,\delta}}{s_i}. \quad (55)$$

Based on this representation for χ^2 (designated as “fitting method II”), we explored the impact of the scale dependence on the constraint on a_Z . Even if the scales are varied, data prefer a nonzero nonperturbative Gaussian smearing of about the same magnitude as in method I.

In the simplest possible case, the $C_{1,2,3}$ parameters are independent of the rapidity or other kinematic parameters and shared by all e and μ bins. In this case, variations of the scale

Fit results for $\phi_\eta^* \leq 0.1$				
C_1, C_2, C_3 are shared by all y_Z bins				
	N_{pt}	χ_{min}^2/N_{pt}	$\bar{a}_Z \pm \delta a_Z$ (GeV ²)	Best-fit $C_{1,2,3}$
All y_Z bins	60	1.29	$0.82^{+0.34}_{-0.12}$	1.4, 0.33, 1.23
		1.31	$0.82^{+0.22}_{-0.11}$	1.42, 0.33, 1.23
C_1, C_2, C_3 are independent in each y_Z bin				
	N_{pt}	χ_{min}^2/N_{pt}	$\bar{a}_Z \pm \delta a_Z$ (GeV ²)	Best-fit $C_{1,2,3}$
$ y_Z \leq 1, e + \mu$	24	1.0	$0.56^{+0.95}_{-0.02}$	0.21, 0.18, 7.56
		1.16	$0.85^{+0.3}_{-0.15}$	1.47, 0.3, 1.46
$1 \leq y_Z \leq 2, e + \mu$	24	1.48	$1.22^{+0.27}_{-0.36}$	18, 0.58, 0.1
		1.70	$0.79^{+0.2}_{-0.1}$	1.69, 0.37, 0.77
$ y_Z \geq 2, e$	12	-	-	-
		0.59	$0.99^{+0.99}_{-0.31}$	1.74, 0.48, 2.12
Weighted average of all bins	60		0.97 ± 0.25	
			0.82 ± 0.12	

Table 2: The best-fit χ^2/N_{pt} , central value and 68% C.L. intervals for a_Z , and best-fit $C_{1,2,3}$ for $1/\sigma_\lambda = 0$ (upper rows in each section) and 1 (lower rows).

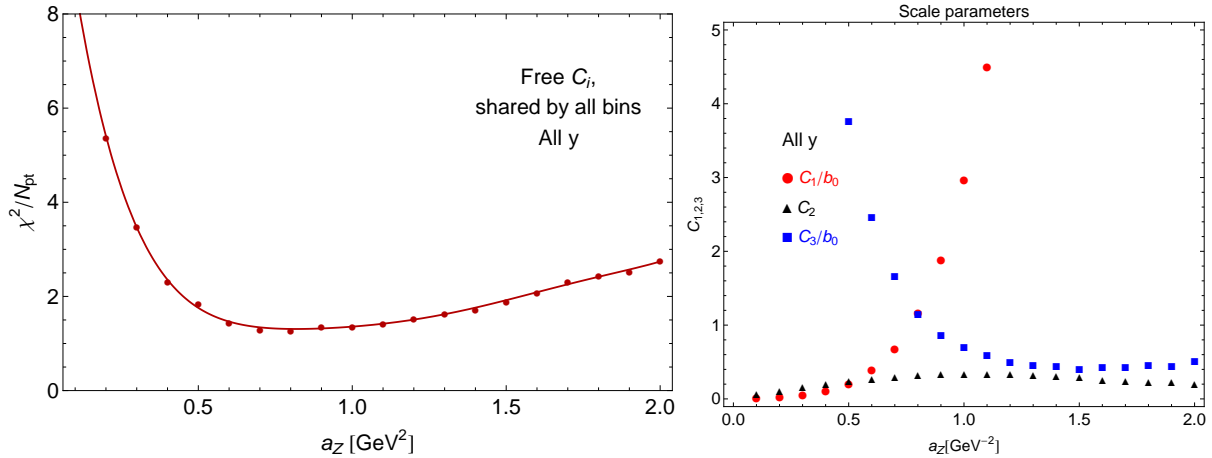


Figure 7: χ^2/N_{pt} and scale parameters as a function of a_Z for $\bar{C}_1 = \bar{C}_3 = 2 b_0, \bar{C}_2 = 1/2$. The scale parameters are shared across three y_Z bins.

parameters reduce χ^2/N_{pt} to about 1.3, *i.e.* the fit is better than for the fixed scale combinations discussed above. We focus on the case when the central scale parameters are $\bar{C}_1 = \bar{C}_3 = 2 b_0, C_2 = 1/2$, although the conclusions remain the same for other choices.

The plots of χ^2/N_{pt} vs. a_Z and optimal $C_1/b_0, C_2, C_3/b_0$ vs. a_Z , derived from the optimal λ_α parameters in Eq. (55), are shown in Fig. 7. The χ^2 dependence on a_Z becomes asymmetric when the scale shifts are allowed, with the large- a_Z branch being flattened out in contrast to the small- a_Z one that remains steeply growing. From the right inset, we see that the optimal C_1 and C_3 are monotonously increasing and decreasing as functions of a_Z , respectively. In the vicinity of the minimum, C_1 and C_3 are of about the same magnitude at $(1.2-1.5)b_0$. Very small or large a_Z can be obtained only by taking C_1 and C_3 to be uncomfortably far from unity. In contrast, the optimal C_2 parameter is generally in the range 0.3-0.5 and has weaker dependence on a_Z .

The values of $\chi^2/N_{pt}, a_Z$, and $C_{1,2,3}$ parameters at the minimum are reported in the upper portion of Table 2. When the $C_{1,2,3}$ parameters are shared by all bins, the fit is relatively insensitive to the confidence level assigned to the variations $\lambda_\alpha \pm 1$, controlled by the parameter σ_λ in Eq. (51). In Table 1, the upper rows in each section correspond to the fit without a constraint on the λ parameters, *i.e.*, for $1/\sigma_\lambda = 0$. The lower rows are for assigning a 68% probability to the $-1 \leq \lambda_\alpha \leq 1$ intervals, corresponding to $1/\sigma_\lambda = 1$.

For the shared $C_{1,2,3}$, the outcomes of the fits with $1/\sigma_\lambda = 0$ and 1 are very similar, apart from the uncertainty on the a_Z parameter, which is increased when the λ_α variations are totally

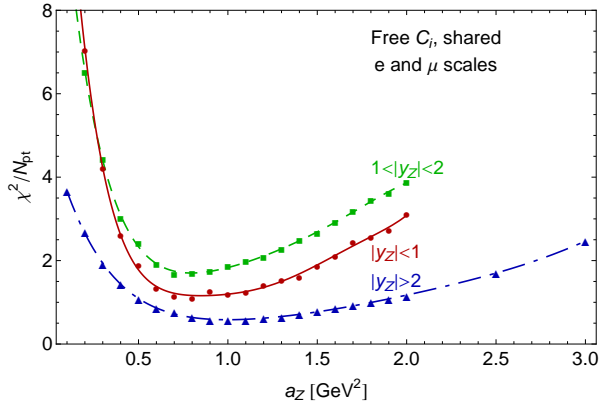


Figure 8: χ^2/N_{pt} as a function of a_Z for $\bar{C}_1 = \bar{C}_3 = 2b_0, \bar{C}_2 = 1/2$. The scale parameters are independent in each y_Z bin.

free. [The asymmetric 68% C.L. uncertainties are computed according to Eq. (48)].

In contrast, when the scale parameters are taken to be independent in each y_Z bin (but still shared between the electron and muon samples), only the case of $\sigma_\lambda = 1$ results in an acceptable fit in all three y_Z bins. The best-fit parameters for this case are listed in the lower part of Table 2. When the scale shifts were arbitrary ($1/\sigma_\lambda = 0$, upper lines), the fits were underconstrained and produced inconsistent a_Z values and large scale shifts in all three bins, especially in the third bin that is not shown for this reason. On the other hand, for $\sigma_\lambda = 1$ (lower lines), the three fits converged well and rendered compatible a_Z values. The χ^2/N_{pt} vs. a_Z dependence for this case is illustrated in Fig. 8, where the minima are neatly aligned in the three bins. The fit to the second bin is generally worse than for the other two, suggesting possible rapidity dependence of a_Z . The scale dependence in each bin is qualitatively similar to that in the right inset of Fig. 7.

Even when $C_{1,2,3}$ are independent in each y_Z bin, by averaging the a_Z values over three bins, we obtain the $\bar{a}_Z = 0.8 - 0.9 \text{ GeV}^2$ in the last section of Table 2 that is essentially the same as in the case when $C_{1,2,3}$ are shared by all bins. The findings in Tables 1 and 2 are recapitulated in Fig. 9, showing the 68% C.L. intervals in the fits with fixed $C_{1,2,3} = b_0, 1/2, b_0$ and $2b_0, 1/2, 2b_0$, as well as the fit with varied $C_{1,2,3}$ and $\sigma_\lambda = 1$. All fits consistently yield a_Z values that are at least 5σ from zero.

4 Implications for the W mass measurement and LHC

The previous sections demonstrated that the ϕ_η^* distributions in Z/γ^* production are sensitive to several QCD effects. Depending on the ϕ_η^* range, hard or soft QCD emissions can be studied.

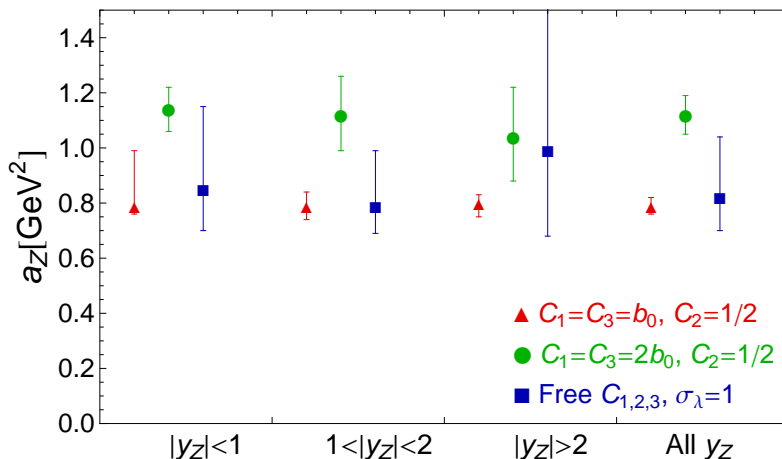


Figure 9: 68% C.L. ranges for a_Z in individual y_Z bins and in all bins.

The nonperturbative power corrections in QCD can be determined at $\phi_\eta^* \leq 0.1$, provided that the dependence on resummation scales is controlled.

To distinguish between various contributing effects, new developments in the Collins-Soper-Sterman resummation formalism were necessitated. The computer code RESBOS includes all such effects relevant for computation of resummed differential distributions of lepton pairs. New components of the theoretical framework implemented in RESBOS were reviewed in Sec. 2. In the large- ϕ_η^* region dominated by hard emissions, the two-loop fixed-order contributions implemented in RESBOS show good agreement with the $D\bar{O}$ data when the renormalization/factorization scale C_4Q for hard emissions is set to be close to $Q/2$.⁶

In the resummed W piece dominating at small ϕ_η^* , we include 2-loop perturbative coefficients in the resummed W term by using the exact formulas for the \mathcal{A} and \mathcal{B} coefficients and a numerical estimate for the small $\mathcal{O}(\alpha_s^2)$ contribution $\delta C^{(2)}$ to the Wilson coefficient functions. We also fully include, up to $\mathcal{O}(\alpha_s^2)$, the dependence on resummation scale parameters C_1 and C_2 , (see Secs. 2.3 and 2.4). Matching corrections and final-state electroweak contributions were implemented and investigated in order to understand their non-negligible impact on the cross sections. Finally, we implemented a form factor $\widetilde{W}_{NP}(b, Q)$ describing soft nonperturbative emissions at transverse positions $b \gtrsim 1 \text{ GeV}^{-1}$ in the context of a two-parameter b_* model [32], cf. Sec. 2.5.

With this setup, we performed a study of the small- ϕ_η^* region at the $D\bar{O}$ Run-2 with the goal to determine the range of plausible nonperturbative contributions. We found that, to

⁶In this region, a three-loop correction must be computed in the future to reach NNLO accuracy in α_s .

describe Drell-Yan dilepton production with the invariant mass $70 \leq Q \leq 110$ GeV, it suffices to use a simplified nonperturbative form factor that retains only a leading power correction, $\widetilde{W}_{NP}(b, Q = M_Z) = \exp(-b^2 a_Z)$. The power correction modifies the shape of $d\sigma/d\phi_\eta^*$ in a pattern distinct from variations due to the dependence on the resummation scales C_1/b , $C_2 Q$, and C_3/b in the leading-power term \widetilde{W}^{pert} , see Figs. 3, 4, and 5. For various fixed combinations of scale parameters $C_{1,2,3}$, or when the scale parameters were varied, the fits require nonzero a_Z values that were summarized in Tables 1 and 2. For example, when the variations in the scales $C_{1,2,3}$ were incorporated as shared free parameters in all rapidity bins using a correlation matrix, we obtained $a_Z = 0.82_{-0.11}^{+0.22}$ GeV² at 68% C.L., cf. Table 2, consistently with the other tried methods. The estimate of the 68% C.L. uncertainty including the scale dependence indicates clear preference for a non-zero a_Z , without appreciable rapidity dependence.

The magnitude of a_Z depends on the resummation scales, but allowing the scales to vary increases the probability for having larger, not smaller a_Z . The best-fit a_Z is also correlated with b_{max} , which controls the upper boundary of the b range where the exact perturbative approximation for $\widetilde{W}^{pert}(b, Q, y_Z)$ is used. Using $b_{max} = 1.5$ GeV⁻¹ in this study, we obtain $a(b, Q) \approx 0.8$ GeV² at $Q = M_Z$, which is consistent with the value obtained with the other \widetilde{W}_{NP} forms maximally preserving the perturbative contribution [74, 75, 76, 32]. The dependence on b_{max} weakens at b_{max} above 1 GeV⁻¹, and even larger a_Z values are preferred for b_{max} below 1 GeV⁻¹, cf. Fig. 2 in [32]. The fitted data was corrected for the effects of final-state NLO QED radiation. In the fitted region $\phi_\eta^* < 0.1$, the uncertainty due to the matching of the resummed and finite-order terms was shown to be negligible.

The nonperturbative form factor at other \sqrt{s} and Q values can be predicted using the relations in Sec. 2.5. This is possible because the dominant part of \widetilde{W}_{NP} is associated with the soft factor $\exp(-S(b, Q))$ which does not depend on \sqrt{s} or the types of the incident hadrons. It is argued in Sec. 2.5 that the \widetilde{W}_{NP} factors are identical within the 68% C.L. error in central-rapidity Z and W production at the same \sqrt{s} . The same a_Z value that we determined can be readily applied to predict W boson differential distributions at the Tevatron Run-2, or, with appropriate modifications proportional to $\ln(Q)$ and $\ln(s)$, in other kinematical ranges, cf. Eq. (38).

The resummation calculation employed in this analysis can be reproduced using the RESBOS-P code [98] and input tables [99] available at the “ Q_T resummation portal at Michigan State University”. The central input tables are provided for $a_Z = 1.12 \pm 0.07$ GeV², $C_1 = C_3 = 2b_0$, $C_2 = 1/2$, and central CT10 NNLO PDF. In addition, the distribution includes RESBOS tables corresponding to the best-fit resummed parameters and CT10 NNLO PDF eigenvector sets.

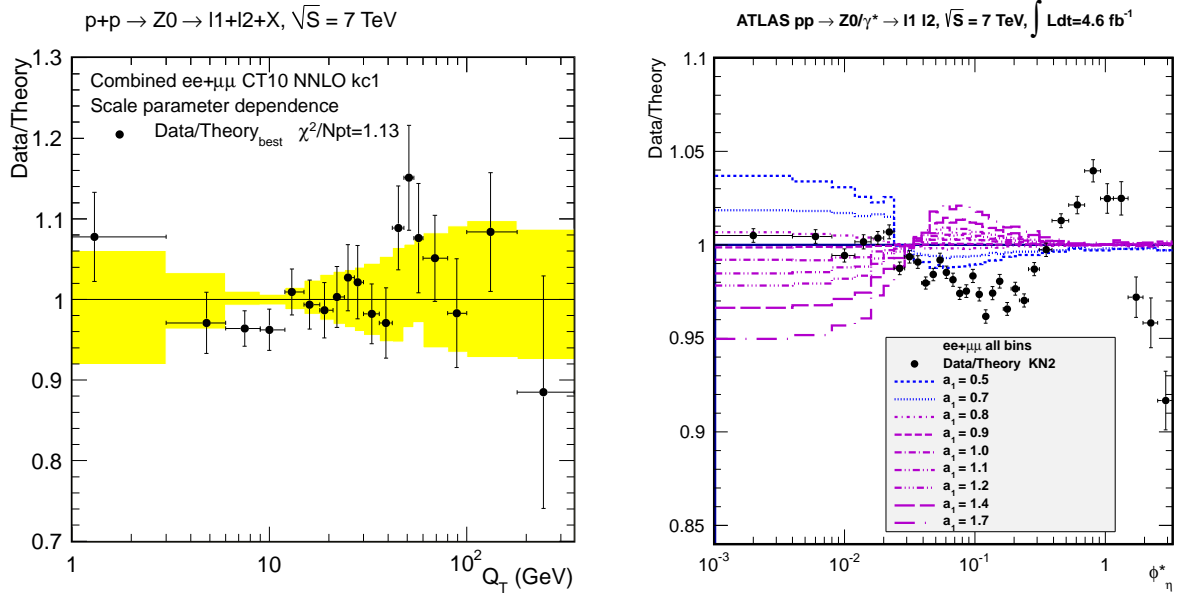


Figure 10: Data vs. theory ratios for the Q_T distribution by ATLAS 7 TeV, $35 - 40 \text{ pb}^{-1}$ [26] and ϕ_η^* distribution ATLAS 7 TeV, 4.6 fb^{-1} [27]

Finally, for a detailed exploration of the low- ϕ_η^* region, the distribution includes tables for a_Z in the interval $0.5 - 1.7 \text{ GeV}^2$ with step 0.1 GeV^2 using the central PDF, and, to study scale dependence, 7 RESBOS grids for the central $a_{Z,central} = 1.12 \text{ GeV}^2$, and the scale parameters $C_1 = b_0, 4b_0$, $C_2 = 1/4, 1$, and $C_3 = b_0, 4b_0$.

As an example of a phenomenological application, Fig. 10 compares the RESBOS predictions with the ATLAS data [26, 27] on Drell-Yan pair production near the Z boson resonance peak at $\sqrt{s} = 7 \text{ TeV}$. The figure shows ratios of data to theory cross sections. The left subfigure shows the Q_T distribution for $35 - 40 \text{ pb}^{-1}$, compared to the RESBOS prediction with $a_Z = 1.1 \text{ GeV}^2$, $C_1 = C_3 = 2 b_0$, $C_2 = 1/2$. The yellow band indicates variations in the cross section due to the scales in the range $C_1 = b_0, 4b_0$, $C_2 = 1/4, 1$, and $C_3 = b_0, 4b_0$. In the case of Q_T distribution, we obtain good agreement between theory and data and in the intermediate/small Q_T region the theoretical uncertainty due to $C_{1,2,3}$ scale parameters is reduced compared to the study of Ref. [20].

The right subfigure shows the ratio of the more recent ϕ_η^* distribution to the central theory prediction based on our default parametrization at much higher level of accuracy. Here, a RESBOS prediction based on the BLNY parametrization has shown better agreement with the data than other available codes and was used for event simulation during the ATLAS analysis.

A comparable, although somewhat worse agreement is realized by the GNW parametrization, which was not used at any stage by ATLAS. The right subfigure shows several curves for the default $C_{1,2,3}$ choice and a_Z in the range $0.5 - 1.7 \text{ GeV}^2$. It is clear that the ATLAS ϕ_η^* data is sensitive to a_Z as well as b_{max} and can possibly discriminate subleading power contributions to the nonperturbative form factor $\widetilde{W}_{NP}(b, Q)$ proportional to b^4 and beyond. We provide sets of updated RESBOS grids for the LHC kinematics that can be used for future improvements in the nonperturbative model.

5 Conclusions

In our analysis we have shown that a significant nonperturbative Gaussian smearing is necessary to describe features of the low ϕ_η^* spectrum. A non-zero NP function is present even if all the perturbative scale parameters of the CSS formalism are varied. Values of a_Z smaller than 0.5 GeV^2 are disfavoured by the fit to the recent $D\bar{O}$ data, as demonstrated in Sec. 3. The dependence of the $d\sigma/d\phi_\eta^*$ on various factors was recently examined in [50], and it was observed that the dependence on the nonperturbative contributions could not be reliably separated from the dependence on the perturbative QCD scales. To go beyond the analysis of Ref. [50], we carried out a quantitative fit to the ϕ_η^* data of $D\bar{O}$, in which we implemented the dependence on the soft resummation scales to NNLO, cf. Sec. 2.4. We found that the small- ϕ_η^* spectrum cannot be fully described by employing perturbative scale variations only. From the characteristic suppression of the production rate at very small ϕ_η^* , or very small Q_T/Q , we established the magnitude of the nonperturbative effects.

The resummed predictions based on the new nonperturbative form are implemented in the RESBOS code. It will be of particular interest to explore the constraining power of the new forthcoming LHC data for Z and W production at a variety of \sqrt{s} , boson's invariant masses, and rapidities. Precise measurements of hadronic cross sections at small Q_T will verify the TMD formalism for QCD factorization and shed light on the nonperturbative QCD dynamics. These developments will depend on consistent combination of NNLO QCD and NLO electroweak effects and reduction of perturbative scale dependence in QCD predictions for Q_T distributions.

Acknowledgments

M.G. and P.N. would like to thank Mika Vesterinen for useful discussion and correspondence, Ted Rogers for his comments on the manuscript, Rafael Lopes de Sà, John Hobbs, and C.-P. Yuan for stimulating discussions. M.G. thanks George Sterman for the hospitality at Stony

Brook University during the 2012 “ $D\bar{O}$ W mass” workshop. M.G. also would like to thank Kostas Theofilatos for discussions on future prospects of the Q_T distribution measurement by the CMS collaboration at the LHC. This work is supported by the U.S. DOE Early Career Research Award de-sc0003870 and by the Lightner Sams Foundation.

References

- [1] P.B. Arnold and M.H. Reno, Nucl.Phys. B319 (1989) 37.
- [2] C. Anastasiou, L. Dixon, K. Melnikov and F. Petriello, Phys.Rev. D69 (2004) 094008, hep-ph/0312266.
- [3] S. Catani, L. Cieri, G. Ferrera, D. de Florian and M. Grazzini, Phys.Rev.Lett. 103 (2009) 082001, 0903.2120.
- [4] G. Bozzi, S. Catani, G. Ferrera, D. de Florian and M. Grazzini, Phys.Lett. B696 (2011) 207, 1007.2351.
- [5] Y.L. Dokshitzer, D. Diakonov and S. Troian, Phys.Lett. B79 (1978) 269.
- [6] G. Parisi and R. Petronzio, Nucl.Phys. B154 (1979) 427.
- [7] G. Curci, M. Greco and Y. Srivastava, Nucl.Phys. B159 (1979) 451.
- [8] J.C. Collins and D.E. Soper, Nucl.Phys. B193 (1981) 381.
- [9] J.C. Collins and D.E. Soper, Nucl.Phys. B197 (1982) 446.
- [10] J.C. Collins, D.E. Soper and G.F. Sterman, Nucl.Phys. B250 (1985) 199.
- [11] J.C. Collins and A. Metz, Phys.Rev.Lett. 93 (2004) 252001, hep-ph/0408249.
- [12] J.C. Collins, Foundations of perturbative QCD (Cambridge University Press, 2011).
- [13] C. Balazs, J. Qiu and C.-P. Yuan, Phys.Lett. B355 (1995) 548, hep-ph/9505203.
- [14] R.K. Ellis and S. Veseli, Nucl.Phys. B511 (1998) 649, hep-ph/9706526.
- [15] D. de Florian and M. Grazzini, Phys.Rev.Lett. 85 (2000) 4678, hep-ph/0008152.
- [16] S. Catani, D. de Florian and M. Grazzini, Nucl.Phys. B596 (2001) 299, hep-ph/0008184.

- [17] D. de Florian and M. Grazzini, Nucl.Phys. B616 (2001) 247, hep-ph/0108273.
- [18] S. Catani and M. Grazzini, Phys.Rev.Lett. 98 (2007) 222002, hep-ph/0703012.
- [19] G. Bozzi, S. Catani, G. Ferrera, D. de Florian and M. Grazzini, Nucl.Phys. B815 (2009) 174, 0812.2862.
- [20] A. Banfi, M. Dasgupta, S. Marzani and L. Tomlinson, Phys.Lett. B715 (2012) 152, 1205.4760.
- [21] A. Banfi, M. Dasgupta and S. Marzani, Phys.Lett. B701 (2011) 75, 1102.3594.
- [22] A. Banfi, M. Dasgupta and R.M. Duran Delgado, JHEP 0912 (2009) 022, 0909.5327.
- [23] P.M. Nadolsky, AIP Conf.Proc. 753 (2005) 158, hep-ph/0412146.
- [24] A. Banfi, S. Redford, M. Vesterinen, P. Waller and T.R. Wyatt, Eur.Phys.J. C71 (2011) 1600, 1009.1580.
- [25] DØ Collaboration, V.M. Abazov et al., Phys.Rev.Lett. 106 (2011) 122001, 1010.0262.
- [26] ATLAS Collaboration, G. Aad et al., Phys.Lett. B705 (2011) 415, 1107.2381.
- [27] ATLAS Collaboration, G. Aad et al., Phys.Lett. B720 (2013) 32, 1211.6899.
- [28] S. Catani, L. Cieri, D. de Florian, G. Ferrera and M. Grazzini, Eur.Phys.J. C72 (2012) 2195, 1209.0158.
- [29] G. Ladinsky and C.-P. Yuan, Phys.Rev. D50 (1994) 4239, hep-ph/9311341.
- [30] C. Balazs and C.-P. Yuan, Phys.Rev. D56 (1997) 5558, hep-ph/9704258.
- [31] F. Landry, R. Brock, P.M. Nadolsky and C.-P. Yuan, Phys.Rev. D67 (2003) 073016, hep-ph/0212159.
- [32] A.V. Konychev and P.M. Nadolsky, Phys.Lett. B633 (2006) 710, hep-ph/0506225.
- [33] J.C. Collins and F. Hautmann, Phys.Lett. B472 (2000) 129, hep-ph/9908467.
- [34] J.C. Collins and F. Hautmann, JHEP 0103 (2001) 016, hep-ph/0009286.
- [35] A. Henneman, D. Boer and P. Mulders, Nucl.Phys. B620 (2002) 331, hep-ph/0104271.

- [36] A.V. Belitsky, X. Ji and F. Yuan, Nucl.Phys. B656 (2003) 165, hep-ph/0208038.
- [37] D. Boer, P. Mulders and F. Pijlman, Nucl.Phys. B667 (2003) 201, hep-ph/0303034.
- [38] J.C. Collins, Acta Phys.Polon. B34 (2003) 3103, hep-ph/0304122.
- [39] J. Collins, T. Rogers and A. Stasto, Phys.Rev. D77 (2008) 085009, 0708.2833.
- [40] A. Idilbi, X.d. Ji and F. Yuan, Phys.Lett. B625 (2005) 253, hep-ph/0507196.
- [41] I. Cherednikov and N. Stefanis, Phys.Rev. D77 (2008) 094001, 0710.1955.
- [42] I. Cherednikov and N. Stefanis, Phys.Rev. D80 (2009) 054008, 0904.2727.
- [43] M.G. Echevarriá, A. Idilbi and I. Scimemi, JHEP 1207 (2012) 002, 1111.4996.
- [44] M.G. Echevarriá, A. Idilbi, A. Schäfer and Ignazio Scimemi,
Eur.Phys.J. C73 (2013) 2636, 1208.1281.
- [45] S.M. Aybat and T.C. Rogers, Phys.Rev. D83 (2011) 114042, 1101.5057.
- [46] T. Becher, M. Neubert and D. Wilhelm, JHEP 1202 (2012) 124, 1109.6027.
- [47] S. Mantry and F. Petriello, Phys.Rev. D83 (2011) 053007, 1007.3773.
- [48] S. Mantry and F. Petriello, Phys.Rev. D84 (2011) 014030, 1011.0757.
- [49] S. Berge, P. Nadolsky, F. Olness and C.-P. Yuan,
Phys.Rev. D72 (2005) 033015, hep-ph/0410375.
- [50] A. Banfi, M. Dasgupta, S. Marzani and L. Tomlinson, JHEP 1201 (2012) 044, 1110.4009.
- [51] J. Collins, Int.J.Mod.Phys.Conf.Ser. 25 (2014) 1460001, 1307.2920.
- [52] P. Schweitzer, M. Strikman and C. Weiss, JHEP 1301 (2013) 163, 1210.1267.
- [53] M. Guzzi and P.M. Nadolsky, Int.J.Mod.Phys.Conf.Ser. 20 (2012) 274, 1209.1252.
- [54] J. Gao, M. Guzzi, J. Huston, H.-L. Lai, Z. Li, P. Nadolsky, J. Pumplin, D. Stump, C.-P. Yuan, Phys.Rev. D89 (2014) 033009, 1302.6246.
- [55] J.C. Collins and D.E. Soper, Phys.Rev. D16 (1977) 2219.
- [56] A. Banfi, M. Dasgupta and Y. Delenda, Phys.Lett. B665 (2008) 86, 0804.3786.

- [57] P.B. Arnold and R.P. Kauffman, Nucl.Phys. B349 (1991) 381.
- [58] J. Kodaira and L. Trentadue, Phys.Lett. B112 (1982) 66.
- [59] J. Kodaira and L. Trentadue, Phys.Lett. B123 (1983) 335.
- [60] C. Davies and W.J. Stirling, Nucl.Phys. B244 (1984) 337.
- [61] C. Davies, B. Webber and W.J. Stirling, Nucl.Phys. B256 (1985) 413.
- [62] S. Catani, E. D’Emilio and L. Trentadue, Phys.Lett. B211 (1988) 335.
- [63] S. Moch, J. Vermaseren and A. Vogt, Nucl.Phys. B688 (2004) 101, hep-ph/0403192.
- [64] T. Becher and M. Neubert, Eur.Phys.J. C71 (2011) 1665, 1007.4005.
- [65] T. Becher, M. Neubert and B.D. Pecjak, JHEP 0701 (2007) 076, hep-ph/0607228.
- [66] T. Becher and M. Neubert, Phys.Rev.Lett. 97 (2006) 082001, hep-ph/0605050.
- [67] T. Becher, M. Neubert and G. Xu, JHEP 0807 (2008) 030, 0710.0680.
- [68] K. Melnikov and F. Petriello, Phys.Rev. D74 (2006) 114017, hep-ph/0609070.
- [69] R. Hamberg, W. van Neerven and T. Matsuura, Nucl.Phys. B359 (1991) 343.
- [70] A. Cafarella, C. Corianò and M. Guzzi, JHEP 0708 (2007) 030, hep-ph/0702244.
- [71] A. Cafarella, C. Corianò and M. Guzzi, Comput.Phys.Commun. 179 (2008) 665, 0803.0462.
- [72] G.P. Korchemsky and G.F. Sterman, Nucl.Phys. B437 (1995) 415, hep-ph/9411211.
- [73] A. Guffanti and G. Smye, JHEP 0010 (2000) 025, hep-ph/0007190.
- [74] J. Qiu and X. Zhang, Phys.Rev. D63 (2001) 114011, hep-ph/0012348.
- [75] S. Tafat, JHEP 0105 (2001) 004, hep-ph/0102237.
- [76] A. Kulesza, G.F. Sterman and W. Vogelsang, Phys.Rev. D66 (2002) 014011, hep-ph/0202251.
- [77] D0 Collaboration, V.M. Abazov et al., Phys.Rev.Lett. 108 (2012) 151804, 1203.0293.
- [78] CDF Collaboration, T. Aaltonen et al., Phys.Rev.Lett. 108 (2012) 151803, 1203.0275.
- [79] G. Bozzi, J. Rojo and A. Vicini, Phys.Rev. D83 (2011) 113008, 1104.2056.

- [80] W.K. Tung, S. Kretzer and C. Schmidt, J. Phys. G28 (2002) 983.
- [81] M. Guzzi, P.Nadolsky, H.-L. Lai and C.-P. Yuan, Phys.Rev. D86 (2012) 053005, 1108.5112.
- [82] G. Bozzi, S. Catani, D. de Florian and M. Grazzini,
Nucl.Phys. B737 (2006) 73, hep-ph/0508068.
- [83] U. Baur , O. Brein, W. Hollik, C. Schappacher and D. Wackerroth,
Phys.Rev. D65 (2002) 033007, hep-ph/0108274.
- [84] V. Zykunov, Phys.Rev. D75 (2007) 073019, hep-ph/0509315.
- [85] C.M. Carloni Calame, G. Montagna, O. Nicrosini and A. Vicini,
JHEP 0710 (2007) 109, 0710.1722.
- [86] A. Arbuzov, D. Bardin, S. Bondarenko, P. Christova, L. Kalinovskaya, G. Nanava and R. Sadykov, Eur.Phys.J. C54 (2008) 451, 0711.0625.
- [87] S. Dittmaier and M. Kramer, Phys.Rev. D65 (2002) 073007, hep-ph/0109062.
- [88] U. Baur and D. Wackerroth, Phys.Rev. D70 (2004) 073015, hep-ph/0405191.
- [89] Q.H. Cao and C.-P. Yuan, Phys.Rev.Lett. 93 (2004) 042001, hep-ph/0401026.
- [90] V. Zykunov, Phys.Atom.Nucl. 69 (2006) 1522.
- [91] A. Arbuzov, D. Bardin, S. Bondarenko, P. Christova, L. Kalinovskaya, G. Nanava and R. Sadykov, Eur.Phys.J. C46 (2006) 407, hep-ph/0506110.
- [92] C.M. Carloni Calame, G. Montagna, O. Nicrosini and A. Vicini,
JHEP 0612 (2006) 016, hep-ph/0609170.
- [93] E. Barberio and Z. Was, Comput.Phys.Commun. 79 (1994) 291.
- [94] S. Catani, L. Trentadue, G. Turnock and B.R. Webber,
Nucl.Phys. B407 (1993) 3.
- [95] A.D. Martin, W.J. Stirling, R.S. Thorne and G. Watt,
Eur.Phys.J. C63 (2009) 189, 0901.0002.
- [96] J. Pumplin, D. Stump, R. Brock, D. Casey, J. Huston, J. Kalk, H.L. Lai and W.K. Tung,
Phys.Rev. D65 (2001) 014013, hep-ph/0101032.

- [97] J. Pumplin, D.R. Stump, J. Huston, H.L. Lai, P.M. Nadolsky and W.K. Tung,
JHEP 07 (2002) 012, hep-ph/0201195.
- [98] http://hep.pa.msu.edu/resum/code/resbos_p/resbos.tar.gz
- [99] http://hep.pa.msu.edu/resum/grids/resbos_p/w_z/tev2/general_purpose/ ;
http://hep.pa.msu.edu/resum/grids/resbos_p/w_z/lhc/general_purpose/